energies

MDPI

Article

Experimental Validation and Performance Benchmarking of a Grid-Connected Rooftop Photovoltaic System Using Measured and Simulated Data

Nuri Caglayan [1,*], H. Kursat Celik [1,2], Filiz Öktüren Asri [3] and Allan E. W. Rennie [2]

[1] Department of Agricultural Machinery and Technology Engineering, Akdeniz University, Antalya 07070, Türkiye; hkcelik@akdeniz.edu.tr
[2] School of Engineering, Lancaster University, Lancaster LA1 4YW, UK; a.rennie@lancaster.ac.uk
[3] Bati Akdeniz Forestry Research Institute, Antalya 07070, Türkiye; filizokturenasri@hotmail.com
* Correspondence: nuricaglayan@akdeniz.edu.tr; Tel.: +90-242-310-6555

Abstract

This study presents a performance and techno-economic evaluation of a 24 kWp grid-connected rooftop photovoltaic system in Yeşilova, Burdur, Türkiye, based on measured operational data from 2024. Beyond conventional software comparisons, this research establishes a validated benchmarking protocol for medium-scale rooftop PV systems by quantifying the divergence between measured data and predictive modeling under fluctuating seasonal conditions. Measured results were compared with energy yield predictions from PVsyst and HelioScope. Key performance indicators, including final yield, performance ratio (PR), and capacity factor, were evaluated alongside main loss components. The system produced an annual energy output of 33,977.5 kWh, corresponding to an average PR of 75.7% and a capacity factor of 16.99%. Simulation results show deviations from measured values, with PVsyst moderately overestimating and HelioScope underestimating the annual yield. Thermal effects were identified as the dominant contributor to performance losses, particularly during elevated summer temperatures. A techno-economic assessment indicates a payback period of 8.4 years, a levelized cost of electricity (LCOE) of 0.0485 US$/kWh, and an internal rate of return (IRR) of 15.58%. These findings underline the importance of validating simulation-based assessments with site-specific measurements to improve the reliability of photovoltaic system performance and investment evaluations.

Keywords: grid-connected photovoltaic system; measured performance analysis; performance ratio; PVsyst; HelioScope; rooftop solar PV

Academic Editor: Michael egnevitsky

Received: 15 February 2026
Revised: 8 March 2026
Accepted: 12 March 2026
Published: 14 March 2026

Copyright: © 2026 by the authors. Licensee MDPI, Basel, Switzerland. This article is an open access article distributed under the terms and conditions of the Creative Commons Attribution (CC BY) license.

1. Introduction

1.1. Solar Energy Outlook in Türkiye: Potential, Current Status, and Strategic Objectives

The persistent growth in global energy demand, coupled with the urgent need to decarbonize energy systems, has positioned solar PV technology at the core of contemporary energy transitions [1–3]. Continuous cost reductions, supportive policy frameworks, and international climate commitments have significantly accelerated global PV deployment. According to the International Energy Agency Photovoltaic Power Systems Programme (IEA-PVPS), cumulative installed solar PV capacity reached approximately 1.6

TW by the end of 2023 and exceeded 2.2 TW in 2024, representing the fastest expansion among all electricity generation technologies [3,4].

Within the European Union, the contribution of solar PV to the renewable electricity mix has intensified substantially. In 2024, wind and solar energy together accounted for nearly 30% of total electricity generation, surpassing fossil fuel-based generation for the first time. Solar PV alone contributed approximately 13% of total electricity production at the EU level [5]. At the national scale, even more pronounced structural shifts are observed, with solar electricity shares exceeding 20% in countries such as Hungary, Greece, and Spain [6]. These developments illustrate the consolidation of decentralized and renewable-oriented electricity systems across Europe.

In this global and regional context, Türkiye occupies a strategically advantageous position within the Mediterranean solar belt. Official statistics from the Ministry of Energy and Natural Resources (MENR) indicate an average annual global solar irradiation of approximately 1527.46 kWh/m^2 and an average annual sunshine duration of about 2741 h [7,8]. These values exceed those of many European countries, offering favorable conditions for high specific yields in PV installations.

The restructuring of Türkiye's electricity sector is primarily driven by the objective of reducing dependence on imported fossil fuels. By early 2026, total installed capacity had reached approximately 122.5 GW [9]. Although coal and natural gas still account for roughly 35–38% of electricity generation, renewable energy sources represent more than 62% of total installed capacity [10]. Among these, solar PV has demonstrated the fastest growth, surpassing 24.8 GW and constituting nearly 20% of total installed capacity [11].

To further accelerate renewable deployment, Türkiye has implemented the Renewable Energy Resource Zone (YEKA) framework, which promotes large-scale projects through competitive auctions designed to enhance cost efficiency and attract private-sector investment [12]. The 2035 Energy Roadmap establishes a strategic target of achieving 120 GW of cumulative installed wind and solar capacity [13]. In parallel, the Turkish National Energy Plan (2020–2035) aims to increase installed solar PV capacity to 52.9 GW by 2035, in alignment with the 2053 net-zero emissions objective [14,15]. Achieving these targets will require sustained annual capacity additions, grid infrastructure expansion, enhanced system flexibility, and advanced operational strategies to manage the increasing penetration of variable renewable energy sources.

Beyond capacity expansion, ensuring the technical reliability of PV systems is equally critical. As solar penetration increases, accurate performance prediction, validation through field measurements, and robust loss analysis become essential for long-term energy planning and investment security. In the last five years, research focusing on the gap between theoretical modeling and real-world performance has intensified, particularly for medium-scale installations. For instance, Ates and Singh (2021) evaluated a 30 kWp rooftop system in Western Turkey (Mediterranean climate) and demonstrated that while simulations align well with annual trends, seasonal deviations in PR can reach significant levels due to localized thermal effects [16]. Similarly, Dindar et al. (2022) conducted a comparative sensitivity analysis of 25 kW systems using PVsyst, PV*SOL, and Solarius, finding that software-to-software discrepancies in energy yield can vary between 5–7%, emphasizing the need for empirical validation against measured field data [17]. Furthermore, recent studies in Mediterranean coastal regions, such as the analysis of grid-connected systems in Alexandria, have highlighted that temperature-induced losses often exceed simulation-based projections by 2–4% during peak summer months [18]. Recent research has therefore shifted toward integrated and optimization-oriented approaches addressing high renewable penetration in distribution networks. These efforts can be broadly categorized into three main research directions: (i) urban PV potential and placement

optimization, (ii) microgrid and energy management system (EMS) architectures with advanced monitoring, and (iii) power quality enhancement and PV power-fluctuation mitigation.

For example, Villa-Ávila et al. [19] proposed the "Roof-Solar-Max" methodology, integrating 3D GIS modeling and Solar Prospet software to optimize rooftop PV placement in complex urban geometries. Their approach enabled accurate quantification of solar self-consumption potential by identifying high-irradiance zones (>1450 kWh/m^2). Similarly, Benavides et al. [20] demonstrated that IoT-based EMS platforms can enhance microgrid stability and power quality through real-time monitoring and automated energy flow management.

While these optimization and supervisory strategies provide advanced architectural solutions, the empirical benchmarking of medium-scale PV systems against widely used industry-standard simulation tools remains comparatively underexplored. Most existing literature in Mediterranean climates either focuses on large-scale utility plants in the MW scale [18] or strictly theoretical assessments providing software-to-software comparisons [17,21]. While some recent studies have begun incorporating measured data for medium-scale systems [16], there is a notable lack of studies that perform a 'triangulated' evaluation combining long-term measured operational data, dual-software simulation (PVsyst vs. HelioScope), and multi-dimensional loss decomposition for a 20–40 kW capacity range. In particular, systematic validation of simulated outputs with long-term measured field data is essential for strengthening confidence in planning tools and reducing uncertainty in performance projections.

1.2. Objectives of This Study

Grid-connected PV systems in the existing literature can generally be classified into three main categories: measurement-based performance evaluations, simulation-based analyses, and techno-economic assessment studies. Despite the aforementioned progress in predictive control and automated monitoring architectures, a significant research gap persists in the quantitative assessment of discrepancies between actual field measurements and simulation-based predictions (e.g., PVsyst and HelioScope) for medium-scale rooftop systems in the Mediterranean climate. The specific contribution of this study lies in its focus on the 24 kWp threshold—a common scale for commercial and agricultural rooftops in the Mediterranean belt—where high ambient temperatures and specific dust patterns often deviate from standard meteorological datasets (e.g., Meteonorm or NASA-SSE) [22,23]. Furthermore, the prolonged arid periods characteristic of the Mediterranean climate exacerbate soiling losses, significantly affecting the annual Specific Yield and PR; yet, the precise quantification of these losses in medium-scale systems remains inconsistent across standard simulation platforms [16,21]. Unlike previous studies that rely on a single simulation tool, this research cross-validates PVsyst and HelioScope against one full year of high-resolution measured data (2024), providing a more granular understanding of loss mechanisms such as temperature-related degradation [16,24] and inverter clipping [17] in this specific climatic context. Accurate and reliable planning of solar PV technologies is of critical importance for maximizing technical performance and ensuring economic sustainability. During system design and planning stages, advanced simulation tools such as PVsyst [25] and HelioScope [26] are widely employed to predict energy generation potential and analyze system losses. Although these software tools have undergone significant development over time, uncertainties in meteorological datasets, modeling assumptions, and site-specific environmental conditions can still lead to considerable discrepancies between simulated outputs and actual operational measurements [27,28]. These discrepancies directly affect the reliability of key performance indicators, including

PR, specific energy yield, and capacity factor, thereby introducing uncertainty into investment decision-making processes.

Simulation-based studies indicate that average specific energy yield and capacity factor values are typically underestimated by approximately 3–10% compared to measured data from installed systems [29,30]. Measurement-based studies reflecting real operating conditions generally report PR values ranging from 73% to 85% [30–32]. In studies conducted in Mediterranean and temperate climates, average PR values are typically reported between 67% and 82%, with seasonal peak values exceeding 90% during winter periods [33,34]. Within the same climatic regions, capacity factor values are most frequently reported within the range of 15–18% [35,36].

Techno-economic analyses conducted using tools such as PVsyst, HOMER, and RETScreen demonstrate that the payback periods of grid-connected PV systems are generally shorter than 5–10 years. Furthermore, system sizing and local electricity tariff structures are identified as the dominant factors influencing economic feasibility [37–39]. However, comprehensive studies simultaneously evaluating measured operational data, simulation-based performance predictions, and techno-economic indicators for the same PV installation remain limited in Türkiye. In particular, there is a significant research gap regarding quantitative assessments of inconsistencies between simulated and measured results for medium-scale grid-connected PV systems, especially in terms of PR, specific energy yield, and major loss components, including irradiance-related losses, temperature effects, soiling, ohmic losses, and inverter losses.

In this context, the present study provides a comprehensive performance evaluation of a 24 kWp grid-connected PV system installed in a region of Türkiye characterized by high solar energy potential. Measured energy production, solar irradiance, and ambient temperature data covering the period from January to December 2024 were utilized to evaluate the prediction accuracy of PVsyst (ver.7.2.4) and HelioScope (Aurora Solar, San Francisco, CA, USA; accessed in 2024) simulation software. The primary objectives of this study are:

i. to quantify deviations between measured and simulated performance indicators, including PR, array yield, and final yield;
ii. to determine the relative contributions of major loss mechanisms in percentage terms;
iii. to assess the techno-economic feasibility of the system through comparison with findings reported in the existing literature.

The methodological approach adopted in this study follows a structured sequence beginning with system characterization and data acquisition, followed by simulation-based performance assessment, loss component decomposition analysis, and techno-economic evaluation. The overall methodological framework is summarized in the flowchart presented in Figure 1.

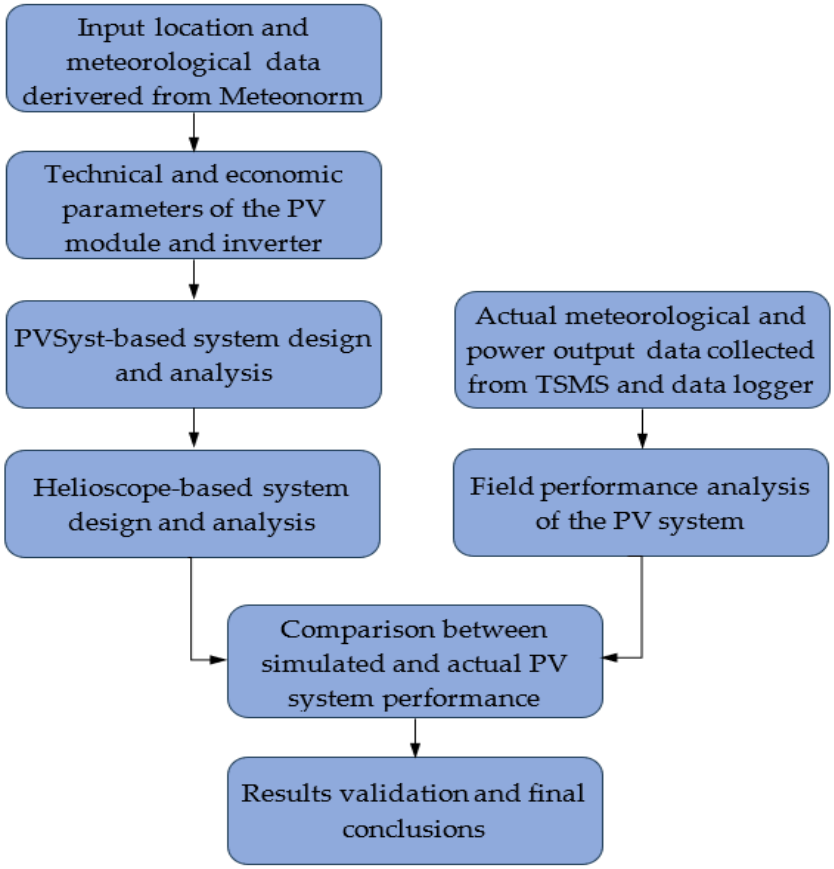


Figure 1. Flowchart.

2. Materials and Methods

2.1. Site and System Design Parameters for Installed PV Array

A 24 kWp grid-connected solar PV system, consisting of 60 solar PV modules, each with a surface area of 2 m² (total installed area of 120 m²), was installed on the rooftop of a building in Yeşilova, Burdur, Türkiye (37.29° N; 29.48° E) (Figure 2).

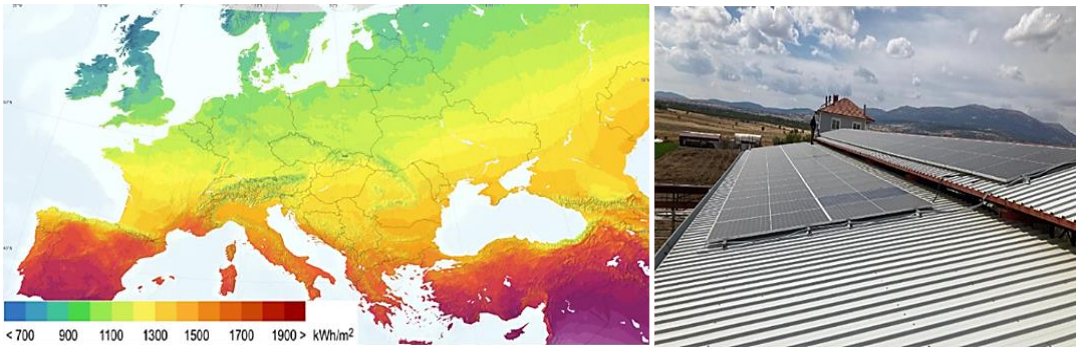


Figure 2. Location map of Yeşilova and a rooftop view of the building on which the PV array is installed. (Map: https://solargis.com/resources/free-maps-and-gis-data?locality=europe (accessed on 17 February 2025), as modified by author).

The system configuration is illustrated in Figure 3, where each string consists of twenty modules connected in series, and three such strings are arranged in parallel. The PV array is installed at a tilt angle of 8°, corresponding to the site's latitude, in order to maximize solar irradiance capture.

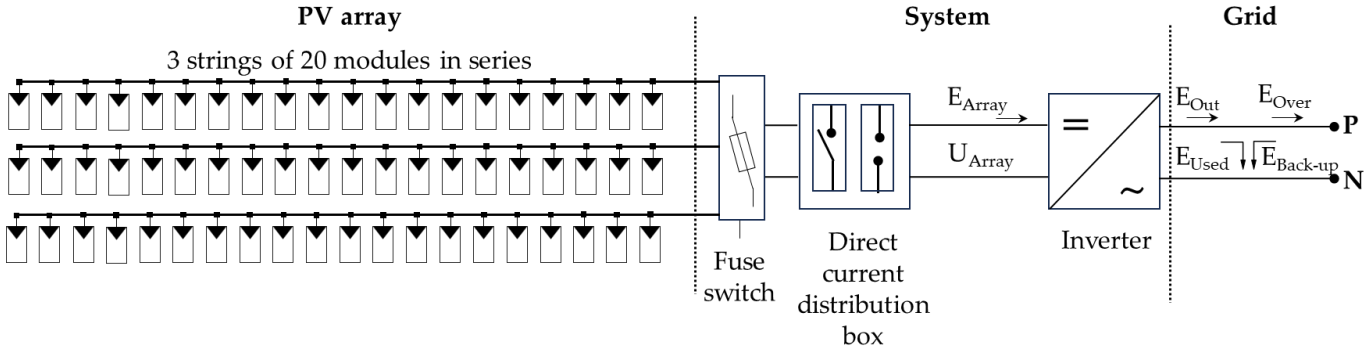


Figure 3. Layout of 24 kWp solar PV system.

The PV system was configured with an array of 60 PV modules (CWT400-72PM-BC, CW, Antalya, Türkiye) and a three-phase 24 kW string inverter for DC–AC conversion (SUN2000-25KTL-ZHM5-380V, Huawei, Shenzhen, China). The detailed technical specifications of the PV modules and the inverter used in this study are presented in Table 1.

Table 1. Technical specifications of the main components.

Component	Technical Specifications
PV Panel	Model: CWT400-72PM-BC, CW Rated capacity: 400 W Panel type: monocrystalline-Si Open circuit voltage (V_{OC}): 49.83 V Short circuit current (I_{SC}): 10.38 A Power tolerance: 0~+5 W Module efficiency: 20.06% Lifetime: 25 years
Inverter	Model: SUN2000-25KTL-ZHM5-380V, Huawei Rated capacity: 25 kW Rated AC output current: 38 A Grid connection form: 3-Phase Max. efficiency: 98.50 Number of MPPT inputs: 2 Transformer: Transformerless Lifetime: 15 years

In this study, the performance of a 24 kWp grid-connected PV system was assessed using a four-step methodology. First, operational data were manually extracted from the monitored PV system. Second, the system performance was simulated using the PVsyst software. Third, an independent performance simulation was carried out using HelioScope. Finally, the measured performance of the PV system was compared with the predicted results obtained from PVsyst and HelioScope.

The technical performance evaluation of the 24 kWp grid-connected PV system relies on high-fidelity, site-specific climate data. Meteorological parameters, including global horizontal irradiance (GHI), wind speed, relative humidity, and precipitation, were obtained from a local weather station situated in the Yeşilova district of Burdur, Türkiye. To ensure maximum reproducibility and capture high-frequency fluctuations, GHI was measured directly on-site at one-minute sampling intervals using a calibrated Delta-T Devices (e.g., model SPN1) pyranometer.

To monitor environmental conditions, ambient air temperature and PV cell temperature were recorded at 15-min intervals using a dedicated data logger (DL2e, Delta-T Devices, Cambridge, UK) equipped with high-precision PT100 sensors (RS Group plc, London, UK). compliant with IEC 60751 Class A standards [40]. In accordance with the IEC 61724-1 monitoring standard [41], these sensors, characterized by an accuracy range of 0.1–0.3 °C and high long-term stability, were utilized to minimize measurement uncertainty at the source. Both ambient and surface temperatures were consistently monitored, and hourly averages were subsequently calculated for the period between 06:00 and 18:00 throughout the monitoring campaign, following the methodology described in [42].

To maintain compatibility with the PVsyst and HelioScope simulation engines, these high-resolution datasets were aggregated into hourly averages for the annual performance modeling. This processing step ensures temporal alignment between the empirical field measurements and the hourly simulation algorithms used by the software tools, providing a robust and high-fidelity baseline for the subsequent validation of energy yield and loss mechanisms.

To ensure data integrity, a standard multi-stage preprocessing procedure was followed. Initially, physical limit filters were applied to identify and exclude outliers, such as irradiance values exceeding 1.2 times the extraterrestrial irradiance, in accordance with the quality assessment criteria proposed by Long and Dutton [43]. Minor data gaps (shorter than 1 h) were resolved using linear interpolation, while any intermittent longer gaps were supplemented with synchronized datasets from the PVGIS database to maintain a continuous and representative annual profile for 2024. All measurements were standardized to Local Standard Time (LST) to ensure synchronization with the simulation tools.

Furthermore, to characterize the impact of PV input variability on system performance, days were classified based on the Daily Clearness Index (K_t) according to the thresholds established by Muneer [44], distinguishing between 'clear-sky' ($K_t > 0.7$) and 'partly cloudy' conditions. The analysis incorporated variability indicators such as the Ramp Rate (RR), following the methodology described by Hoff and Perez [45] calculated at 1-min resolutions. The maximum observed ramp rate reached 420 W/m² min during transitional weather conditions, particularly in the spring months. The maximum observed ramp rate reached 420 W/m² min during transitional weather conditions, particularly in the spring months. This value represents the peak variation in Global Horizontal Irradiance (GHI) and was derived by identifying the maximum absolute difference between consecutive 1-min readings, defined as [45,46],

$$\mathrm{RR_{max}} = \max|\mathrm{GHI_t} - \mathrm{GHI_{t-1}}| \quad (1)$$

In this expression, RR_{max} represents the maximum observed solar ramp rate (W/m² min), while GHI_t and GHI_{t-1} denote the global horizontal irradiance measured at the current and immediately preceding one-minute intervals, respectively. The use of the absolute difference ensures that both sudden cloud-induced drops and rapid clear-sky increases are captured. This phenomenon typically occurs during cloud-edge effects or rapid clearing in transitional seasons, aligning with Mediterranean climatic profiles where sudden shifts (such as a drop from 900 W/m² to 400 W/m²) are physically observed within a single minute. Thus, it provides a strong empirical basis for the assessment of variability-induced losses and performance fluctuations. Additionally, the PV modules were mounted on a metal support structure at a tilt angle of 8°, oriented southward (0° azimuth), and were cleaned at ten-day intervals to mitigate performance degradation associated with soiling.

Simulation Environment and Technical Configuration

To ensure a high-fidelity comparison between the empirical results and simulation outputs, standardized technical parameters were defined across both PVSyst and HelioScope platforms. These settings were selected to reflect the specific operational environment of the 24 kWp system in Yeşilova. A constant albedo of 0.2 was assumed for the surrounding terrain, and a soiling loss factor of 3% was applied based on the ten-day cleaning cycle mentioned previously. The thermal behavior was modeled using a loss coefficient of 20 W/m²K, consistent with rear-ventilated rooftop installations. Near-shading conditions were integrated via 3D scene modeling of the rooftop, while the horizon was considered unobstructed. The detailed configuration parameters used in the annual energy modeling are summarized in Table 2.

Table 2. Technical parameters and loss configurations used in PVsyst and HelioScope simulations.

Parameter	Value/Assumption
Albedo Coefficient	0.2 (Standard for mixed environments)
Soiling Loss	3.0% (Annual average)
Thermal Loss Coefficient (Uc)	20 W/m²K (Fixed-mounting, ventilated)
Module Mismatch Loss	2.0%
Ohmic Wiring Loss (DC/AC)	1.5%/1.0%
LID (Light Induced Degradation)	2.0%
Horizon Profile	Free-horizon (0° elevation)
Shading Conditions	Near-shading based on 3D geometry (No far-shading)

2.2. Performance Parameters

In PV power plants, energy losses are unavoidable and originate from various sources. These losses may result from environmental conditions such as operating temperature, soiling, and ambient humidity [47,48], as well as from system components and electrical interconnections, including inefficiencies in maximum power point tracking (MPPT), module mismatch, inverter losses, and ohmic losses in cabling [49,50]. To systematically evaluate the operational performance of the PV plant and to quantify the contribution of different loss mechanisms, the performance parameters were calculated in accordance with the IEC 61724-1 standard, which establishes the methodology for assessing energy yield, system losses, capacity factor, and PR under real operating conditions [41].

2.2.1. Array Yield

Array yield defines the ratio of energy generated by the array as direct current to the nominal rated power of the PV plant. It represents how many hours a day the array operates at maximum power to generate energy. It is calculated as [51]:

$$Y_a = \frac{E_{dc}}{P_{rated}} \quad (2)$$

where Y_a: array yield (h/d), E_{dc}: dc electricity generation of the array (kWh/d) and P_{rated}: the rated power of the PV plant (kWp).

2.2.2. Reference Yield

Reference yield is required in terms of hours needed at the reference irradiance level to obtain instantaneous irradiation. Reference yield is calculated theoretically as [51]:

$$Y_r = \frac{H_t}{G_0} \quad (3)$$

where Y_r: reference yield (h/d), H_t: the solar irradiation on the module plane (kWh/m²·d) and G_0: the irradiation corresponding to the Standard Test Condition (STC) (1000 W/m² at 25 °C).

2.2.3. Final Yield

The final yield is the ratio of generating energy from the PV plant as net AC energy to the rated power of the PV plant at STC [51].

$$Y_f = \frac{E_{ac}}{P_{rated}} \quad (4)$$

where Y_f: final yield (h/d) and E_{ac}: AC electricity generation (kWh/d).

2.2.4. Performance Ratio

The PR (%) quantifies the cumulative impact of all system losses on the PV installation and serves as an indicator of how closely the system operates relative to an ideal, loss-free PV system [52]. It is expressed as follows:

$$PR = \frac{Y_f}{Y_r} \quad (5)$$

The acceptable range of PR of the grid-connected PV system varies from 60 to 80% [53].

2.2.5. Capacity Factor

The capacity factor (CF, %) represents the proportion of the energy generated by a power plant over a defined period relative to its theoretical maximum energy output under continuous full-capacity operation. For most power plants, typical capacity factor values generally fall within the range of 10% to 25% [54].

$$CF = \frac{E_{ac}}{P_{rated} \times 24 \times 30} \quad (6)$$

2.2.6. Inverter Efficiency

Inverter efficiency is expressed as the ratio of the AC energy supplied to the grid to the DC energy produced by the PV array. It can be calculated as follows [49]:

$$\eta_{inv} = \frac{E_{ac}}{E_{dc}} \quad (7)$$

2.2.7. System Efficiency

The overall efficiency of a PV system is the measurement of how much of the available solar energy is converted into usable AC electrical energy. It is defined as the ratio of AC energy supplied to the grid to the solar energy coming to the module plane, and is calculated as [55]:

$$\eta_{syst} = \frac{E_{ac}}{H_t \times A_{PV}} \quad (8)$$

where A_{PV}: the total area of the PV array (m²).

2.2.8. Thermal Capture Loss

Thermal capture losses refer to the energy losses resulting from PV cell temperatures exceeding the standard reference value of 25 °C. These losses are quantified as the difference between the reference yield and the temperature-corrected reference yield and can be expressed as follows [42].

$$L_{CT} = Y_r - Y_{cr} \quad (9)$$

where L_{CT} represents the thermal capture losses, expressed in hours per day (h/d).

To account for the impact of module operating temperature on power output under real operating conditions, the temperature-corrected reference yield is defined as follows [56]:

$$Y_{cr} = Y_r[1 + \gamma(T_{cell} - T_{ref})] \quad (10)$$

where γ denotes the module maximum power temperature coefficient (1/°C), T_{cell} represents the average cell temperature (°C), and T_{ref} is the reference cell temperature, set to 25 °C. The average cell temperature can be calculated using Equation (10) [24].

$$T_{cell} = T_{air} + \left(\frac{NOCT - 20}{800}\right) G \quad (11)$$

where T_{cell} denotes the cell temperature (°C) and T_{air} represents the ambient temperature (°C). NOCT denotes the nominal operating cell temperature defined under standard reference conditions of solar irradiance G = 800 W/m², an ambient temperature of 20 °C, and a wind speed of 1 m/s.

2.2.9. System Loss

System losses encompass all energy losses that occur throughout the process of converting the DC energy generated by the PV array into usable AC energy. These losses can be quantified as follows [57]:

$$L_S = Y_a - Y_f \quad (12)$$

where L_S represents the system loss, expressed in hours per day (h/d).

2.2.10. Miscellaneous Capture Loss

Losses arising from low irradiance levels, shading effects, dust deposition on modules, mismatch, and wiring are grouped as miscellaneous capture losses. These losses are determined by subtracting the array yield from the corrected reference yield, as expressed in Equation (13) [58]:

$$L_{CM} = Y_{cr} - Y_a \quad (13)$$

where L_{CM} represents the miscellaneous capture loss, expressed in hours per day (h/d).

Shading Loss

The output power of PV modules significantly decreases due to partial or complete shading on the module surface. In polycrystalline silicon modules, bypass diodes are integrated to mitigate such efficiency losses caused by shading and to prevent the formation of hot spots [53]. Furthermore, shading losses occur due to distant objects on the horizon, particularly during sunrise and sunset when the sun is at a low elevation. These shading losses are directly dependent on the solar position, which is primarily defined by the solar altitude angle (α) and the azimuth angle (γ), as illustrated in Figure 4.

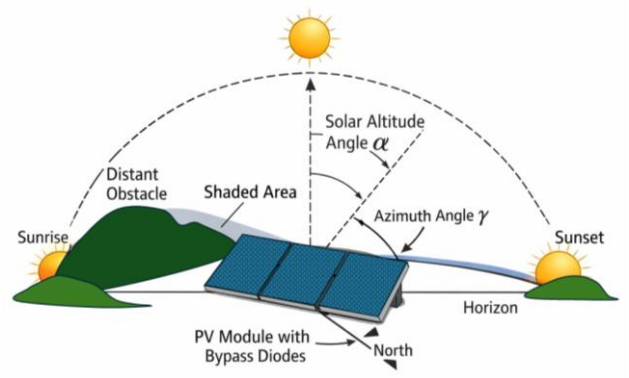


Figure 4. Schematic illustration of the solar position (altitude and azimuth angles), shading effects on a PV module, and the role of bypass diodes in mitigating power losses and hotspot formation. Source: Author-generated.

Soiling Loss

Dust accumulation on the surface of PV modules adversely affects overall efficiency and energy yield. According to the literature, annual losses due to soiling vary between 1.5% and 6.2%, depending on the geographical location of the PV plant [49]. Generally, soiling loss factors are accepted as 2% for low-pollution environments and 8% for high-pollution conditions [59].

The calculation of soiling loss (S_L) based on short-circuit current comparison is a well-established procedure in the literature [60–64]. As described in the methodology, this approach provides a reliable metric for assessing the degradation of optical transmittance caused by surface contamination (Equation (14)) [60].

$$s_L = \left[1 - \frac{I_{sc,\,soiled}}{I_{sc,\,cleaned}}\right] \times 100 \quad (14)$$

where S_L denotes the soiling loss percentage (%), $I_{sc,soiled}$ represents the short-circuit current measured under soiled surface conditions (A), and $I_{sc,cleaned}$ corresponds to the short-circuit current of the same PV module after being thoroughly cleaned (A).

In this study, power losses resulting from dust accumulation were quantified using measured field data. The maximum voltage (V_m) and maximum current (I_m) values of both clean and soiled reference modules were measured simultaneously with solar irradiance. Data collection was conducted daily at solar noon (12:00) over a period of 10 consecutive days. Following this 10-day observation period, the PV modules were regularly cleaned to mitigate soiling losses and restore performance levels.

Mismatch Loss

Mismatch losses occur when PV modules with non-identical current–voltage (I–V) characteristics are integrated into a single array, resulting in a total power output that is less than the theoretical sum of the individual modules' capacities [65]. Even modules from the same manufacturer and rating may exhibit these discrepancies due to inherent variations in the manufacturing process and batch-to-batch differences [66]. Consequently, these electrical inconsistencies lead to a significant reduction in the overall efficiency of the PV system, a phenomenon formally defined as mismatch loss [67].

Ohmic Loss

Ohmic losses in PV systems represent the power dissipation resulting from the electrical resistance encountered by the charge carriers within the cell and the external circuitry. This phenomenon is primarily attributed to the resistance of the bulk

semiconductor material, the contact resistance between the semiconductor and metal electrodes, and the cumulative resistance of the busbars and interconnecting cables. The power loss due to Ohmic resistance is expressed in Equations (15) and (16):

$$P_{ohmic} = I^2 \times R_s \quad (15)$$

$$R_s = \rho \frac{L}{A} \quad (16)$$

where P_{ohmic} denotes the power dissipation in Watts (W), I represents the operating current of the PV module in Amperes (A), and R_S corresponds to the total series resistance of the system expressed in Ohms (Ω), as shown in Equation (15). This relationship underscores the critical impact of series resistance on the overall fill factor and conversion efficiency of the PV device [68,69].

Furthermore, Ohmic losses in PV installations are directly proportional to the total conductor length, as extended cable distances enhance electrical resistance within the DC circuitry. In the present study, the DC wiring consists of a copper conductor with a cross-sectional area (A) of 4 mm^2 and a single-run length (L) of 36.17 m. To determine the associated resistive losses, the electrical resistivity of copper (ϱ) was taken as 1.68×10^{-8} Ω.m [70].

2.3. Economic Parameters

2.3.1. Levelized Cost of Energy

Levelized Cost of Energy (LCOE) is defined as the ratio between the life-cycle cost of the PV system to the whole-life produced energy [71] as shown in Equation (17).

$$LCOE = \frac{\text{Life Cycle Cost (LCC)}}{\text{Life Cycle Energy produced (LCE)}} \quad (17)$$

Life cycle cost (LCC) is an analytical approach used to estimate the total cost of a project over its entire lifetime, taking into account initial investment costs, fuel expenditures, operation and maintenance costs, repair and replacement costs, residual value, financing charges, and other relevant economic considerations. The life cycle cost can be determined using Equation (18) [72].

$$LCC = C_I + C_{OMR} + C_{rep} + C_o - C_{res} \quad (18)$$

This cost is influenced by several factors such as investment cost (C_I), operating cost, maintenance and repair (C_{OMR}), replacement cost (C_{rep}), other costs (C_o), and residual value (C_{res}).

The Life Cycle Energy (LCE) produced can then be calculated on an annual basis and discounted with *r*, as shown in Equation (19).

$$LCE = \sum_{i=0}^{n} \frac{AEP \times (1 - df)i}{(1 - r)i} \quad (19)$$

Here, AEP denotes the expected annual energy production over the projected lifetime of the system, while *r* represents the interest rate. As the system ages, its power output gradually decreases; therefore, a degradation factor (df) is incorporated to provide a more accurate estimation of long-term energy generation [73].

2.3.2. Net Present Value

Net Present Value (NPV) represents the difference between the present value of incoming cash flows and outgoing cash flows over a specified period [71]. A positive NPV indicates a financially viable investment, whereas a negative NPV suggests a potential net loss. The NPV is calculated [74] using Equation (20):

$$NPV = -C_0 + \sum_{i=1}^{t} \frac{C_i}{(1+r)^i} \quad (20)$$

Here, C_0 represents the initial investment cost, C_i denotes the annual cash flows, r is the discount rate, and *t* corresponds to the system's total operational lifetime expressed in years.

2.3.3. Return on Investment

Return on Investment (ROI) represents the proportion of the net economic gain generated by a system relative to the total capital invested. It is typically expressed as a percentage (%) and serves as a key indicator for assessing the economic feasibility and financial performance of PV system investments. The ROI can be calculated as follows [75]:

$$ROI = \frac{\text{NetProfit}(\text{Total Economic Benefit} - \text{Total System Cost})}{\text{Total Investment Cost}} \times 100 \quad (21)$$

where Net Profit represents the difference between the total economic benefits generated by the PV system (such as electricity cost savings or revenues from energy sales) and the total system costs over the assessment period. The Total Investment Cost includes the initial capital expenditure (CAPEX) and, when applicable, operation and maintenance costs.

2.3.4. Sensitivity Analysis and Economic Assumptions

The economic viability of the 24 kWp grid-connected PV system was evaluated using a robust financial framework designed to ensure the reliability of life-cycle cost indicators. A real discount rate of 10% was adopted as a proxy for the Weighted Average Cost of Capital (WACC) typically observed in the Turkish renewable energy sector. This rate accounts for the country-specific risk premium, the cost of equity, and the opportunity cost associated with distributed generation investments. To maintain rigorous internal consistency, all financial evaluations were conducted in real terms (constant prices). By utilizing a real discount rate, the analysis inherently neutralizes the distorting effects of long-term inflation on cash flows. Meanwhile, an underlying annual inflation rate of 2% was assumed for operational and maintenance expenses, aligning with International Energy Agency (IEA) benchmarks.

To further enhance the practical value and decision-making utility of the study, a comprehensive sensitivity analysis was performed to quantify the impact of inherent uncertainties in key technical and economic parameters on the Levelized Cost of Electricity (LCOE) and Net Present Value (NPV). Within this scope, the discount rate was varied between 8% and 12% to reflect potential fluctuations in the cost of capital and macroeconomic stability, while the feed-in tariff was simulated with a ±20% variance to account for potential regulatory shifts in self-consumption incentives and grid-sell rates in Türkiye. Furthermore, the annual degradation rate was adjusted within a range of 0.4% to 0.8%—against a baseline of 0.5%—to evaluate long-term performance risks associated with the high ambient temperatures of the Mediterranean climate, which may accelerate the thermal aging of PV modules. This multi-parametric approach ensures that the economic findings provide a risk-aware perspective for stakeholders and investors rather than remaining as static projections. The results of the sensitivity analysis revealed that while the LCOE is most sensitive to variations in the discount rate, the payback period is primarily influenced by fluctuations in the feed-in tariff.

2.4. Simulation by PVSyst Software

PVSyst is a widely used simulation software for the performance analysis of PV systems. It enables the estimation of system losses, energy yield, and PR, thereby supporting comprehensive technical and economic assessments of PV installations. The performance

simulation of the grid-connected PV system, conducted via PVSyst software, indicates that the maximum power output is achieved in July, whereas the minimum occurs in December (Table 2). Owing to a higher array yield of 4689 kWh in July, the energy supplied to the grid peaked at 4417 kWh; conversely, the lower array yield of 1793 kWh in December resulted in a minimum grid injection of 1690 kWh. The annual total horizontal irradiation was calculated at 1800.2 kWh/m^2, slightly exceeding the measured value of 1603.7 kWh/m^2 while the total incident energy on the collector plane was determined to be 1908.2 kWh/m^2. The total annual energy generation from the PV panels was found to be 39,154 kWh, and the total energy supplied to the grid was 36,049 kWh, which is marginally higher than the recorded measurement of 33,977.50 kWh. Annual ohmic losses and other systemic losses were quantified at 562.94 kWh and 852.2 kWh, respectively. Consequently, the estimated average PR of the system was calculated as 78.7%, surpassing the empirical measurement of 75.7%.

An analysis of the system's energy production profile indicates that daily energy output reaches maximum values of approximately 170 kWh during June and July, while declining to seasonal minimum levels in the November–December period (Figure 5). This trend reflects a typical solar irradiance and energy production pattern for a region located in the Northern Hemisphere. Nevertheless, the daily production curve is characterized by pronounced high-frequency fluctuations rather than a smooth, idealized trajectory.

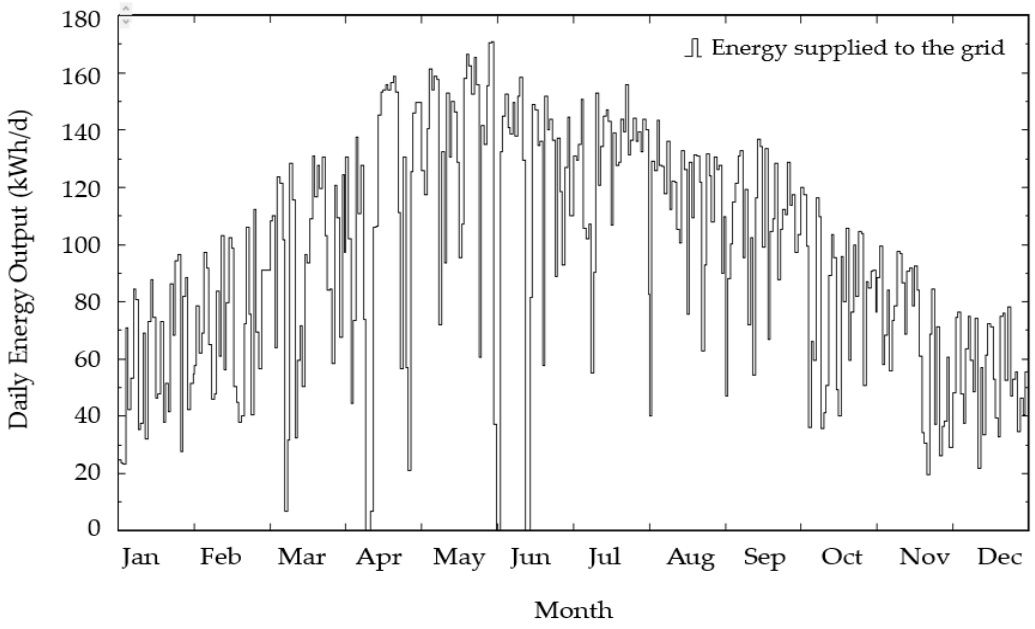


Figure 5. Daily system energy output predicted by PVSyst.

In particular, the abrupt production drops and sharp variations observed during March, April, and May highlight the instantaneous impact of short-term variability in local meteorological conditions on PV system performance. Moreover, it is plausible that part of this variability may originate from the quality and resolution of the meteorological input data.

The PVsyst simulation framework provides a statistical assessment that extends beyond single-year energy yield predictions by explicitly accounting for long-term uncertainties. Each data point in the daily production profile corresponds to the P50 scenario, representing the most probable energy yield. For investment and risk assessment purposes, P90 values, defined as the energy level expected to be exceeded with a 90% probability, are also calculated. As the dispersion of daily production values increases, the uncertainty associated with annual energy yield estimates correspondingly rises, directly

influencing financial risk evaluations. In this context, the high variability observed during the March–May period may be considered a relatively high-risk interval for investors and should therefore be carefully incorporated into cash flow projections.

Accordingly, the daily energy production profile generated by PVsyst serves not only as a performance indicator, but also as a strategic diagnostic tool that reflects both design quality and exposure to environmental risks. The pronounced production drops observed during the spring months further suggest the need to reassess site-specific operation and maintenance strategies to mitigate performance variability.

Conversely, an examination of the July and August period reveals that, despite the highest levels of solar irradiance, daily energy outputs occasionally remain below the peak values observed in April. This phenomenon can be attributed to thermal-induced performance degradation, whereby elevated ambient and cell temperatures reduce module efficiency. Increasing cell temperatures diminish conversion efficiency even under high-irradiance conditions, thereby partially suppressing the expected summer production gains.

In the context of Türkiye's climatic conditions, particularly in the Mediterranean region where the system is installed, thermal performance degradation effects are especially pronounced due to the simultaneous occurrence of high solar irradiance and elevated ambient temperatures during the summer months. Several studies focusing on PV system performance in Türkiye have reported that module operating temperatures frequently exceed 60 °C under peak summer conditions, resulting in substantial power losses associated with the negative temperature coefficients of crystalline silicon modules [76,77]. Under these conditions, the energy gains from increased irradiance are partially or even fully offset by temperature-induced efficiency reductions. Consequently, thermal derating emerges as a critical performance-limiting factor for grid-connected PV systems in Türkiye and should be explicitly incorporated into system design considerations, technology selection, and long-term energy yield and risk assessments.

The operational losses of the system are detailed in Figures 6 and 7 and Table 3, in accordance with the PVSyst outputs. The normalized production analysis indicates that the capture losses stand at 0.76 h/d, while the system losses are at the level of 0.35 h/d. In light of these parameters, the final energy yield of the system was recorded as 4.12 h/d.

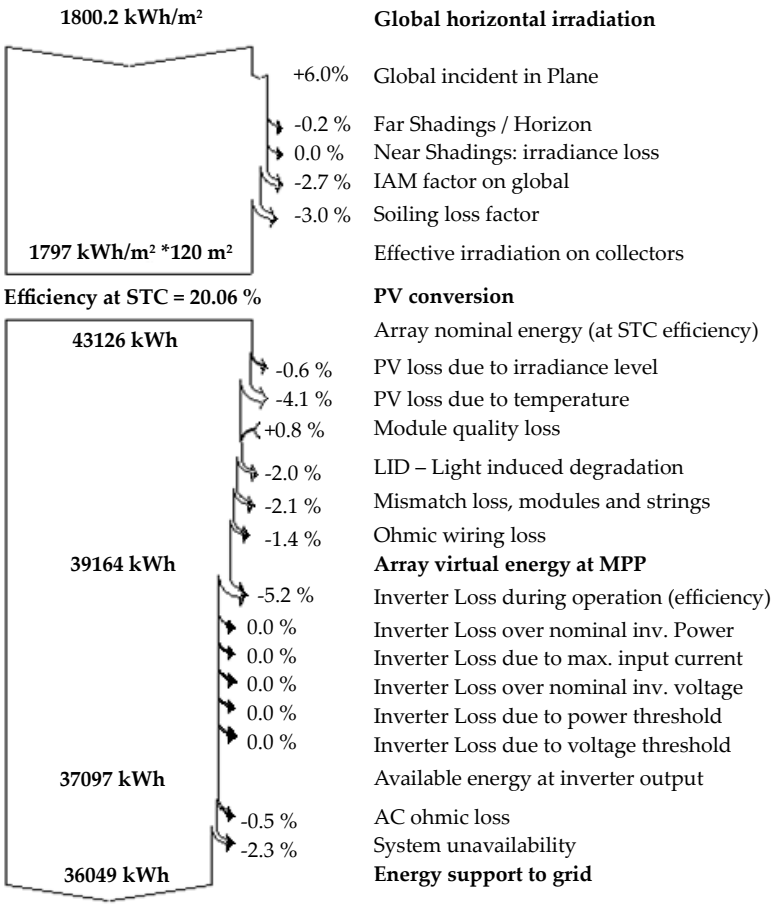


Figure 6. Predicted loss by PVSyst.

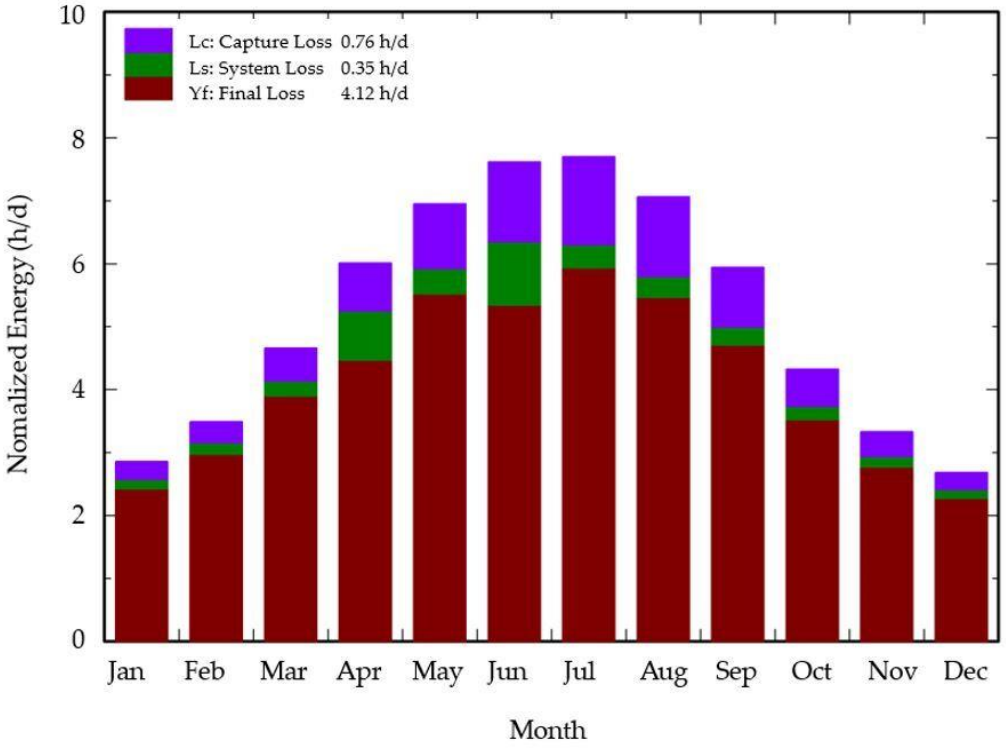


Figure 7. Normalized Energy Production per Installed kWp for the 24 kWp PV System.

Table 3. Meteonorm-Based Performance Balances and Key Results.

Month	GlobHor (kWh/m²)	T_{amb} (°C)	GlobInc (kWh/m²)	E_{array} (kWh)	E_{grid} (kWh)	OhmLoss (kWh)	MisLoss (kWh)	InvLoss (kWh)	PR (%)
Jan	75.1	3.39	88.5	1916	1804	17.87	41.5	104.5	84.9
Feb	87.3	4.83	97.8	2120	1998	21.60	45.9	112.9	85.1
Mar	133.6	8.43	144.4	3078	2900	38.48	66.9	162.7	83.7
Apr	173.3	12.31	180.3	3781	3217	55.59	82.3	198.8	74.3
May	212.4	17.36	215.5	4406	4106	71.79	96.2	241.2	79.4
Jun	228.5	22.33	228.5	4572	3845	77.14	99.8	242.6	70.1
Jul	237.1	26.91	238.8	4689	4417	81.54	102.3	245.3	77.1
Aug	211.8	26.88	218.9	4312	4067	72.46	94.1	221.0	77.4
Sep	166.1	21.32	178.3	3595	3390	54.21	78.3	185.2	79.2
Oct	119.8	15.15	134.0	2779	2622	34.35	60.4	144.1	81.5
Nov	85.6	9.35	99.9	2114	1993	22.18	45.8	112.2	83.1
Dec	69.7	5.05	83.2	1793	1690	15.74	38.8	96.7	84.6
Year	1800.2	14.50	1908.2	39,154	36,049	562.94	852.2	2067.2	78.7

2.5. Simulation by HelioScope Software

HelioScope is a cloud-based PV system design and performance simulation platform developed by the U.S.-based company Folsom Labs [26]. The software supports the detailed design of grid-connected PV systems by incorporating site-specific geographical information, such as latitude and longitude, corresponding to the intended installation location. When accurate site data are combined with appropriate selection of PV modules, inverters, and transformers, HelioScope provides detailed forecasts of system performance, including expected power output, energy injected into the grid, the number of modules installed, and array configuration. These outputs allow for a comprehensive evaluation of the proposed PV system design [78].

In this study, the grid-tied PV system was modeled using HelioScope, which allows the use of meteorological inputs obtained either from the Turkish State Meteorological Service (TSMS), offering location-specific climate data for areas such as Yeşilova, or from the Meteonorm database. The selection of these meteorological datasets was governed by three main criteria: geographical precision, ensuring the TSMS ground station (2 km proximity) accurately captured the site's micro-climate; methodological benchmarking, using Meteonorm as a synthetic baseline to evaluate typical modeling uncertainties; and temporal synchronization, ensuring all data corresponded exactly to the 2024 monitoring period. By integrating these meteorological datasets with the electrical characteristics of the selected PV modules and inverters, the software generates detailed performance estimates. Simulation results based on TSMS data reveal that electricity generation reaches its peak during the summer months, with the highest output recorded in July, followed by August and June, whereas the lowest energy production occurs in February (Table 4).

Table 4. HelioScope simulation results based on TSMS data.

Month	Global Horizontal Irradiance (kWh/m²)	Plane of Array Irradiance (kWh/m²)	E_{grid} (kWh)	Annual Average PR (%)
Jan	69.4	77.5	1525.7	76.4
Feb	62.1	65.9	1307.8	
Mar	130.5	138.5	2662.6	
Apr	155.4	158.1	2968.3	
May	191.5	193.7	3541.7	
Jun	214.5	215.4	3840.4	
Jul	226.3	228.6	4005.6	
Aug	215.5	220.8	3839.7	

Sep	165.4	173.5	3136.6
Oct	124.8	133.8	2483.1
Nov	83.8	93.1	1773.8
Dec	64.1	71.3	1391.7
Total	1703.3	1770.2	32,477

The annual global horizontal irradiance was determined to be 1703.3 kWh/m², whereas the irradiance incident on the collector plane reached 1770.2 kWh/m². Throughout the operational period from January to December, the cumulative energy supplied to the grid totaled 32,477 kWh. The estimated average annual PR of the PV system was calculated as 76.4%, surpassing the empirically measured value. Furthermore, the average operating cell temperature derived from the simulation was 39.1 °C (Table 5), which is notably lower than the recorded in situ measurement of 42.8 °C.

Table 5. Annual production details by HelioScope.

Parameters	Description	TSMS		Meteonorm	
		Output	Relative Difference (%)	Output	Relative Difference (%)
Irradiance (kWh/m²)	Annual global horizontal irradiance	1703.3		1665.8	
	In-plane irradiance	1770.2	3.9	1705.6	2.4
	Shaded irradiance	1770.2		1705.6	
	Irradiance after reflection	1705.2	−3.7	1640.9	−3.8
	Irradiance after soiling	1671.1	−2.0	1608.1	−2.0
	Total collector irradiance	1671.1		1608.1	
Energy (kWh)	Nameplate	40,136.3		38,622.0	
	Output at irradiance levels	39,847.3	−0.7	38,578.3	−0.1
	Output at cell temperature derate	35,376.4	−11.2	34,590.1	−10.3
	Output after mismatch	34,378.8	−2.8	33,614.7	−2.8
	Optimal DC output	34,206.9	−0.5	33,449.6	−0.5
	Constrained DC output	34,138.5	−0.2	33,449.6	
	Inverter output	32,465.7	−4.9	31,810.6	−4.9
	Energy to grid	32,173.5	−0.9	31,544.0	−0.8
Temperature (°C)	Average operating ambient temperature	17.7		15.9	
	Average operating cell temperature	39.1		34.8	

Losses

Figure 8 presents the energy loss diagram generated by HelioScope using TSMS-based meteorological data. As reported in Table 5, thermal-related derating constitutes the dominant loss mechanism, accounting for 11.2% of the total energy reduction. Optical losses due to soiling are estimated at 2.0%, while electrical mismatch losses contribute an additional 2.8%. No energy loss is attributed to shading, as no shading effects were considered in the system configuration. Losses associated with irradiance-level effects remain marginal at 0.7%, remaining below the 1% threshold. In addition, inverter conversion results in a 4.9% efficiency loss, which is in close agreement with both the manufacturer's datasheet specifications and the measured performance. Finally, the comparative assessment of TSMS- and Meteonorm-based results presented in Table 5 indicates that simulations driven by TSMS solar irradiance data yield consistently higher energy production estimates than those derived from Meteonorm datasets.

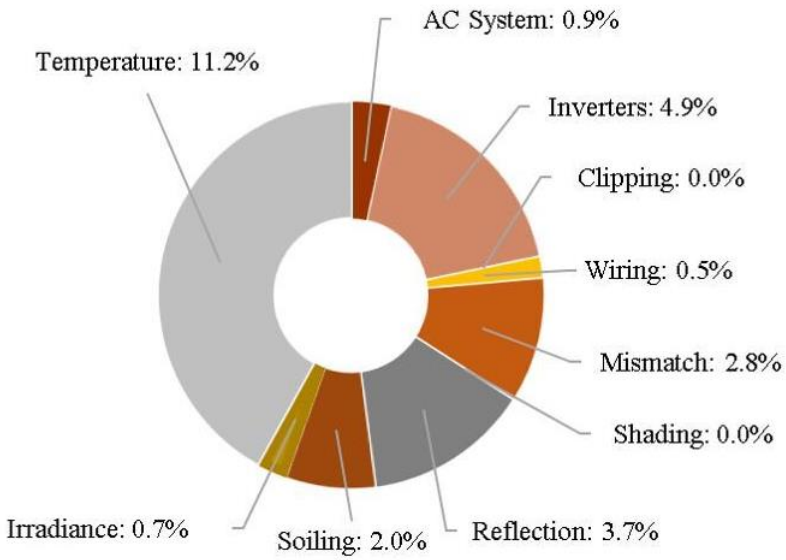


Figure 8. HelioScope–TSMS-based system loss diagram.

The closer agreement between the energy yield results derived from TSMS data and the measured values can primarily be attributed to the temporal differences between the datasets. While the Meteonorm data used for the Yeşilova site are based on an older reference period (1981–1990), the TSMS dataset relies on more recent climatological normals covering the 1991–2020 period, which constitutes the main source of discrepancy between the two datasets. This comparison clearly demonstrates the direct influence of climate variability and long-term changes on energy yield projections.

2.6. Model Validation and Performance Comparison Criteria

The predictive accuracy of the PVsyst and HelioScope models was validated through a direct empirical comparison with the measured AC energy production from the 24 kWp system. The validation procedure involved synchronizing the monthly energy yield data recorded by the inverter monitoring system with the simulation outputs for the period from January to December 2024. To ensure a high-fidelity comparison and data integrity, the operational logs were carefully reviewed; periods of recorded grid instability or scheduled maintenance were identified to ensure the comparative analysis reflects standard operating conditions. The models were evaluated based on their ability to replicate seasonal generation trends and the relative percentage deviation between actual and predicted annual yields, providing a transparent benchmark for software performance in Mediterranean climatic conditions.

3. Results

3.1. Weather Data

Hourly wind speed, precipitation, and relative humidity data, along with ten-minute solar radiation measurements obtained from the Yeşilova local meteorological station throughout the full year of 2024 (January–December), were analyzed. The DC and AC power outputs of the PV system were recorded via the Huawei FusionSolar cloud platform. For simulation purposes, long-term weather data from Meteonorm were utilized in PVSyst, while both TSMS and Meteonorm datasets were employed in HelioScope.

In 2024, the highest measured average temperature on site was recorded in July at 24.6 °C, while the lowest average was 2.5 °C in January (Table 6). In contrast to the temperature-dependent losses predicted by simulation software based on historical long-term averages, the measured losses were derived from actual field conditions. A relatively low

annual average temperature of 13.3 °C was recorded during 2024, the year the study was conducted. This low temperature value is attributed to the high number of rainy and cloudy days, recorded as 88 days. The highest precipitation amounts were recorded in January (56.6 mm) and December (60.3 mm), whereas the lowest precipitation was observed in August (9.5 mm). This circumstance constitutes the primary reason for the observed discrepancies between the simulated and measured results.

Table 6. On-site recorded meteorological data.

Month	Ambient Temperature			Wind Speed	Relative Humidity	Precipitation Amount	Number of Precipitation Days
	Max	Min	Mean	(km/h)	(%)	(mm)	
Jan	6.7	−0.9	2.5	7.3	78	56.6	11
Feb	8.8	−0.3	3.8	8.8	75	41.2	10
Mar	12.6	1.9	6.8	9.6	68	45.1	10
Apr	17.8	6.1	11.7	9.2	50	42.2	9
May	23.1	10.2	16.5	7.8	56	45.2	10
Jun	28.0	14.0	21.0	7.3	60	29.7	6
Jul	32.0	17.0	24.6	9.5	38	13.0	3
Aug	32.2	16.9	23.9	8.5	54	9.5	2
Sep	27.9	12.9	20.2	7.6	43	15.6	3
Oct	21.5	8.4	14.5	8.9	59	31.9	6
Nov	14.5	4.1	8.8	9.6	64	36.1	7
Dec	8.5	0.9	4.3	10.3	81	60.3	11
Average	19.5	7.6	13.3	8.70	60.5	35.53	7.3

3.2. Measured Performance of the Grid-Connected Rooftop PV System

The operational performance parameters of the PV system are categorized in Table 7. The analysis shows that the highest final yield (5.61 h/d), reference yield (7.36 h/d), and array yield (7.01 h/d) were achieved in July, whereas the maximum PR (83%) was recorded in February.

During the monitoring period, the annual average PR of the system was determined to be 75.7%**.** This value corresponds to a higher performance level than those reported for comparable PV systems. As an example of these studies, Pietruszko and Gradzki [79] calculated the PR of the solar energy system as 60–80% in their study. Similar performance rates were also obtained in other studies; 74% [80], 76% [81], 77.5% [82], 78% [83], 78,1% [84] and 79.5% [85] ratios were obtained.

An examination of the individual loss contributions indicates that the thermal capture loss amounts to 0.31 h/day, while miscellaneous capture losses are estimated at 0.22 h/day. In addition, the overall system loss is evaluated as 0.45 h/day. As presented in Table 7, efficiency- and loss-related parameters are reported as annual mean values expressed in h/day, whereas energy-related indicators are given as cumulative annual totals. The negative miscellaneous capture losses observed between May and September are primarily attributed to uncertainties in cell temperature estimation based on a NOCT-derived methodology, which is known to exhibit limitations under real outdoor operating conditions [24,86]. Moreover, during summer periods characterized by high irradiance levels and large angles of incidence, potential inaccuracies in plane-of-array irradiance measurements may further exacerbate these discrepancies [87]. In line with previous studies, several investigations suggest that miscellaneous capture losses may, in certain cases, assume negative values within the associated uncertainties, without necessarily implying a physical performance gain [88,89].

Table 7. Performance Analysis of a 24 kWp Grid-Connected PV System Based on Measured Data.

Month	In-Plane Irradiance (kWh/m²·d)	Yield (h/d)			PR (%)	ηsyst (%)	Losses (h/d)				CF (%)	E_{grid} (kWh)	Edc (kWh/m²·d)	Eac (kWh/m²·d)
		Yf	Yr	Ya			L_{CT}	L_{CM}	L_C	L_S				
Jan	3.01	2.22	3.01	2.44	73.9	14.78	0.03	0.54	0.57	0.22	9.25	1654.90	58.66	53.38
Feb	3.62	2.99	3.62	3.36	82.7	16.54	0.06	0.20	0.26	0.37	12.46	2010.80	80.69	71.81
Mar	4.59	3.64	4.59	4.14	79.3	15.86	0.12	0.33	0.45	0.50	15.17	2708.70	99.29	87.38
Apr	6.27	4.74	6.27	5.88	75.6	15.12	0.29	0.10	0.39	1.14	19.75	3413.80	135.47	113.79
May	6.68	5.19	6.68	6.32	77.7	15.53	0.44	−0.08	0.36	1.13	21.63	3858.10	151.77	124.45
Jun	7.07	5.43	7.07	6.63	76.9	15.37	0.59	−0.15	0.44	1.20	22.63	3912.60	159.05	130.42
Jul	7.36	5.61	7.36	7.01	76.2	15.25	0.72	−0.37	0.35	1.40	23.38	4173.60	168.29	134.63
Aug	6.51	4.96	6.51	6.20	76.2	15.24	0.62	−0.31	0.31	1.24	20.67	3688.40	148.73	118.98
Sep	5.40	4.29	5.40	5.17	79.4	15.88	0.44	−0.21	0.23	0.88	17.88	3087.70	124.00	102.92
Oct	4.14	3.06	4.14	3.60	73.8	14.76	0.24	0.30	0.54	0.54	12.75	2273.90	86.30	73.35
Nov	3.74	2.61	3.74	2.97	69.8	13.95	0.13	0.64	0.77	0.36	10.88	1880.60	71.23	62.69
Dec	2.63	1.77	2.63	1.92	67.1	13.41	0.05	0.66	0.71	0.15	7.38	1314.40	46.09	42.40
Annual average	5.09	3.88	5.09	4.64	75.7	15.14	0.31	0.22	0.45	0.76	16.99	2831.46	110.80	93.02

3.3. Economic Analysis Methodology

All economic calculations were performed in US$. A long-term inflation rate of 2% was adopted in line with commonly accepted assumptions used by the Federal Reserve and the International Energy Agency (IEA). Accordingly, nominal discount rates were employed in the cash flow analysis. A real discount rate of 10% was assumed; therefore, no additional inflation adjustment was applied to the cash flows. In accordance with the recommendations of IEA-PVPS and the National Renewable Energy Laboratory (NREL), an annual PV module degradation rate of 0.5% per year was considered in the analysis. The project lifetime was assumed to be 25 years. The feed-in tariff was taken as 0.075 US$/kWh in real terms and was assumed to be guaranteed for a period of 10 years. After the expiration of the tariff warranty period, electricity revenues were estimated based on prevailing market prices. These assumptions were used to evaluate the long-term economic performance and financial viability of the PV system.

3.4. Economic Results

The breakdown of the installation costs for the PV system is presented in Table 8. The total initial investment was calculated as US$14,014.75, with PV modules accounting for the largest share of the capital expenditure. Specifically, 60 modules represented an investment of US$5075, corresponding to approximately 36% of the total system cost. The costs associated with the mounting structures and the inverter were US$1760 and US$1387.90, respectively. Additional balance-of-system components, including wiring, accessories, and the combiner box, constituted essential expenditures to ensure safe, reliable, and long-term system operation. Installation and labour costs amounted to US$2640, representing nearly 19% of the overall investment. The annual operating costs of the system are summarized in Table 9. The total operating expenditure was estimated at US$395.29 per year, covering routine maintenance, repair activities, and provisions for inverter replacement.

A comprehensive financial evaluation of the PV system is reported in Table 10. Based on the adopted assumptions, the payback period was calculated to be 8.4 years. The NPV and IRR were determined as US$4938.75 and 15.58%, respectively, indicating the economic feasibility of the proposed installation. Furthermore, the LCOE was calculated as US$0.0485/kWh, demonstrating that the system is economically competitive with conventional grid electricity. The cumulative cash flow over the project lifetime is illustrated in

Figure 9, which shows a positive cash flow after the payback period, thereby further confirming the long-term financial viability of the investment.

Table 8. Installation costs.

Item	Quantity	Cost (US$)	Total (US$)
CWT400-72PM-BC	60	84.58	5075.00
Supports for modules	60	29.33	1760.00
Huawei SUN2000-25KTL-ZHM5-380V	1	1387.90	1387.90
Accessories, fasteners	1	15.00	15.00
Wiring	1	436.85	436.85
Combiner box	1	2700.00	2700.00
Installation cost	60	44.00	2640.00
Total			14,014.75
Depreciable asset			7537.90

Table 9. Annual operating costs.

Item	Total (US$/Year)
Repairs	216.00
Provision for inverter replacement	92.53
Operating costs (incl. inflation 2.00%/year)	395.29

Table 10. Financial analysis.

Simulation Period	
Project lifetime	25 years
Inflation	2.00%/year
Production variation (aging)	0.50%/year
Discount rate	10.00%/year
Own funds	14,014.75 US$
Feed-in tariff	0.0750 US$/kWh
Duration of tariff warranty	10 years
Feed-in tariff decrease after warranty	50%
Payback period	8.4 years
Net present value (NPV)	4938.75 US$
Internal rate of return (IRR)	15.58%
Return on investment (ROI)	35.2%
Cost of produced energy (LCOE)	0.0485 US$/kWh

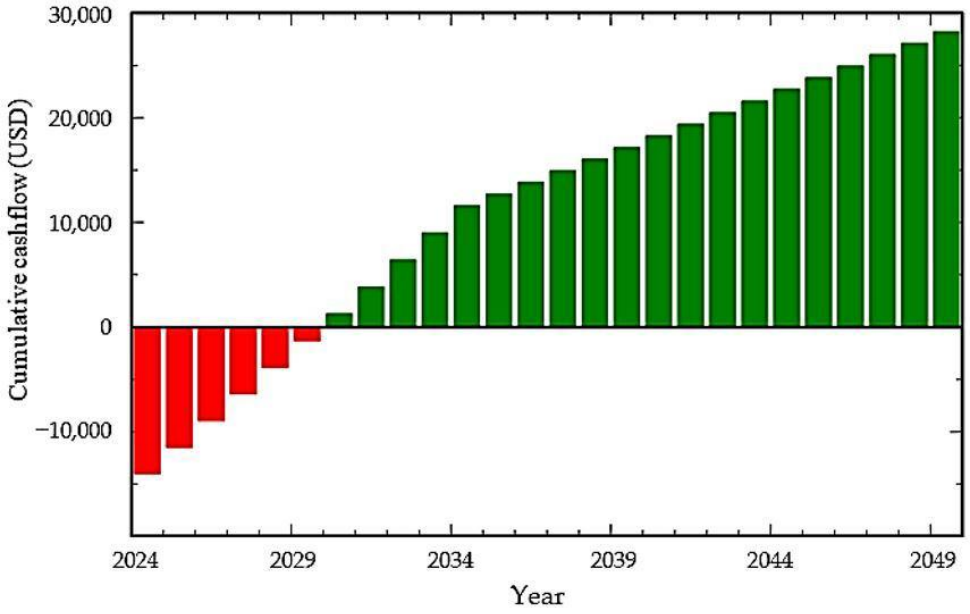


Figure 9. Cumulative cashflow (US$).

3.5. Environmental Impact

Over the operational lifetime of the PV system, a net reduction of approximately 298 tCO_2 in greenhouse gas emissions is achieved. The emissions associated with the manufacturing, installation, and operational phases of the system were estimated to be 38.01 tCO_2, whereas the emissions avoided through electricity generation amounted to 369 tCO_2. Considering an annual energy production of 37.74 MWh and a grid emission factor of 489 gCO_2/kWh, these results demonstrate that the system provides a substantial contribution to greenhouse gas mitigation and underline the environmental benefits of grid-connected PV systems, in accordance with the sustainability objectives of renewable energy deployment.

3.6. Comparison of Measured Performance with Simulated Values

Figure 10 illustrates the daily total plane-of-array (POA) solar irradiance alongside the measured and long-term average ambient temperatures. Comparative results indicate that the measured ambient temperatures are consistently lower than the Meteonorm-derived data generated by PVsyst. The temperature deviations range from a minimum of 0.5 °C in November to a maximum of 2.98 °C in August. Conversely, excluding the first quarter (January–March), no significant discrepancies were observed between the measured data and the HelioScope estimates based on TSMS data. The deviation between HelioScope and measured values reached its minimum in December (0.05 °C) and its peak in March (1.42 °C).

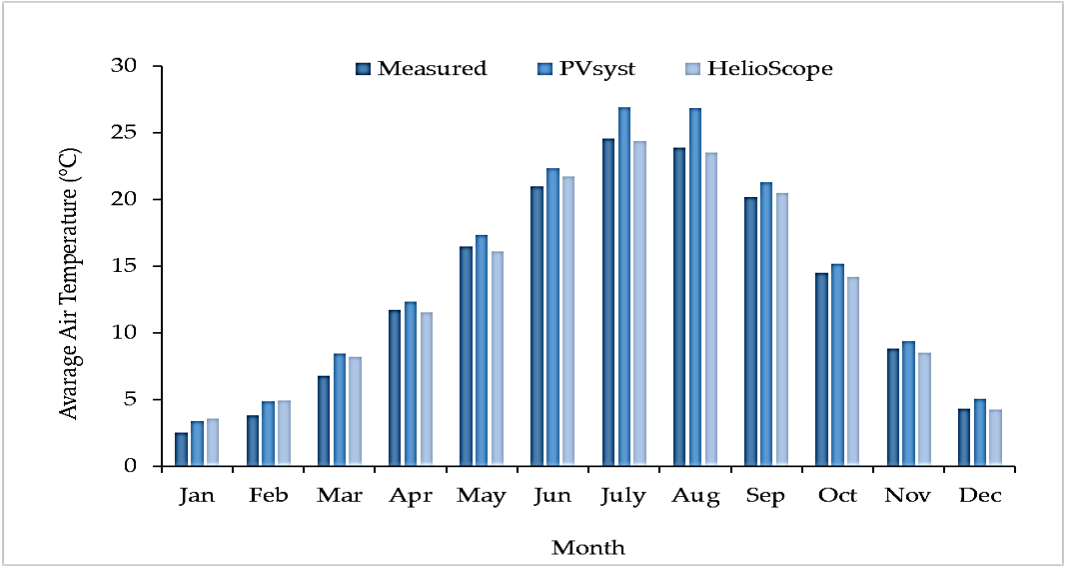


Figure 10. Monthly Average Measured and Long-Term Air Temperature.

The comparison of measured, PVsyst, and HelioScope plane-of-array global solar irradiance values reveals that all datasets exhibit a consistent and pronounced seasonal trend throughout the year (Figure 11). For all methods, the lowest POA irradiance values occur during the winter months, particularly in December and January, whilst the highest values are recorded during the summer period, mainly between June and July. Based on the measured data, the annual maximum POA irradiance was observed in July, reaching 7.46 kWh/m²·d, whereas the corresponding values obtained from PVsyst and HelioScope were 7.70 kWh/m²·d and 7.38 kWh/m²·d, respectively. These results indicate that both simulation tools are generally capable of adequately representing high-irradiance summer conditions.

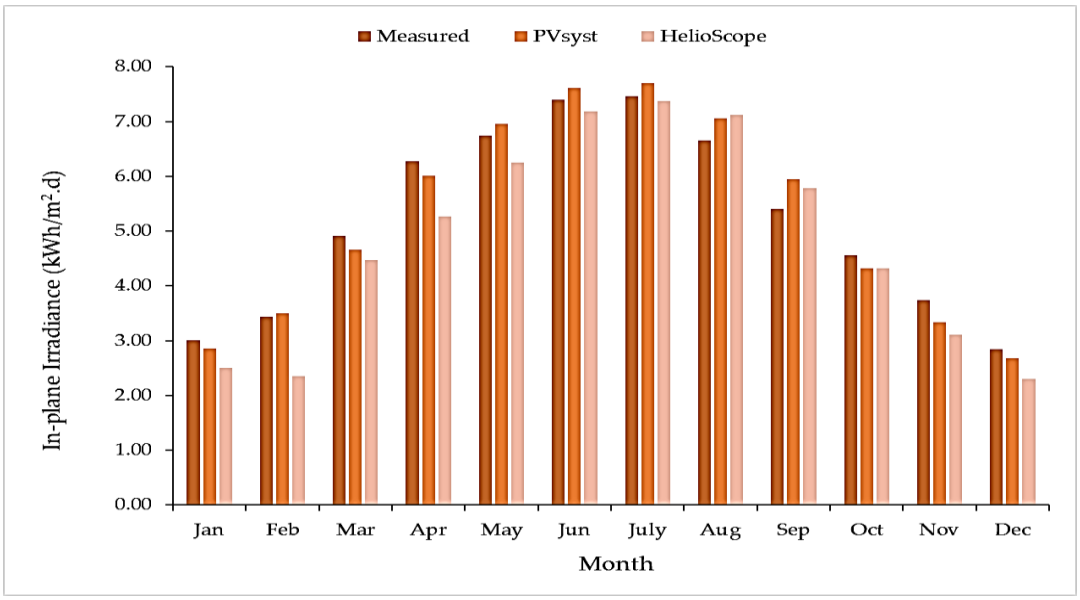


Figure 11. Comparison of measured and long-term average monthly in-plane irradiance.

In contrast, more pronounced discrepancies between the simulated and measured values are observed during the winter months. For instance, in January, the measured POA irradiance amounted to 3.01 kWh/m²·d, while PVsyst and HelioScope underestimated this value by approximately 5.3% (2.85 kWh/m²·d) and 17.0% (2.50 kWh/m²·d), respectively. A similar trend was identified in December, when the measured POA

irradiance of 2.85 kWh/m²·d was compared with PVsyst (2.68 kWh/m²·d) and HelioScope (2.30 kWh/m²·d) outputs. These findings suggest that HelioScope, in particular, tends to systematically underestimate POA irradiance under winter conditions.

During the spring season (March–May), the agreement between simulated and measured values improves noticeably. In March, the measured POA irradiance was 4.91 kWh/m²·d, while PVsyst and HelioScope yielded 4.66 kWh/m²·d and 4.47 kWh/m²·d, corresponding to deviations of approximately 5.1% and 9.0, respectively. In April, the measured value of 6.28 kWh/m²·d was closely reproduced by PVsyst (6.01 kWh/m²·d), whereas HelioScope provided a lower estimate of 5.27 kWh/m²·d. In May, PVsyst slightly overestimated the measured irradiance (6.74 kWh/m²·d) by about 3.1%, while HelioScope underestimated it by approximately 7.3%. Overall, these results demonstrate that PVsyst provides a more consistent representation of measured POA irradiance during the spring months.

In the summer period (June–August), both simulation tools show good agreement with the measured data, although a tendency toward overestimation is observed in certain months. In June, the measured POA irradiance of 7.40 kWh/m²·d was overestimated by PVsyst (7.62 kWh/m²·d, +3.0%) and slightly underestimated by HelioScope (7.18 kWh/m²·d, −3.0%). In August, the measured value of 6.66 kWh/m²·d was exceeded by both PVsyst (7.06 kWh/m²·d) and HelioScope (7.13 kWh/m²·d), corresponding to overestimations of approximately 6.0% and 7.1%, respectively. These discrepancies may be attributed to limitations of long-term meteorological datasets in capturing short-term local atmospheric effects, such as precipitation events or transient cloud cover, which are more frequent during summer months.

During the autumn season (September–November), the simulated values again converge toward the measured data. In September, the measured POA irradiance of 5.40 kWh/m²·d was overestimated by PVsyst (5.94 kWh/m²·d) and HelioScope (5.78 kWh/m²·d) by approximately 10.0% and 7.0%, respectively. In October, the measured value (4.56 kWh/m²·d) was identically estimated by both simulation tools at 4.32 kWh/m²·d, resulting in a deviation of about 5.3%. In November, the measured POA irradiance (3.74 kWh/m²·d) was underestimated by PVsyst (3.33 kWh/m²·d, −11.0%) and HelioScope (3.10 kWh/m²·d, −17.1%).

Overall, PVsyst demonstrates closer agreement with the measured POA irradiance values throughout the year compared to HelioScope, particularly during the spring and summer seasons, where lower deviations are observed. HelioScope, on the other hand, exhibits a more pronounced underestimation tendency during winter months. These differences can be primarily attributed to variations in the meteorological data sources (Meteonorm and TSMS), data resolution, and the irradiance transposition and modeling approaches employed by each simulation tool. The results clearly highlight the importance of validating long-term meteorological datasets with site-specific measurements, especially when conducting monthly and seasonal performance assessments of PV systems.

The monthly average measured and simulated energy supplied to the grid, together with system losses, are presented in Figure 12. When the measured energy production data are compared with the Meteonorm-based PVsyst and HelioScope simulation results, all three datasets exhibit a consistent seasonal pattern characterized by an increase in energy production from winter to summer followed by a gradual decline. The measured energy output increases from 1654.9 kWh in January to a maximum of 4173.6 kWh in July and decreases to 1314.4 kWh in December. For the corresponding months, PVsyst estimates 1804 kWh, 4417 kWh, and 1690 kWh, while HelioScope estimates 1389 kWh, 4009 kWh, and 1225 kWh, respectively. Despite differences in absolute values, both simulation tools successfully capture the annual variation in energy production.

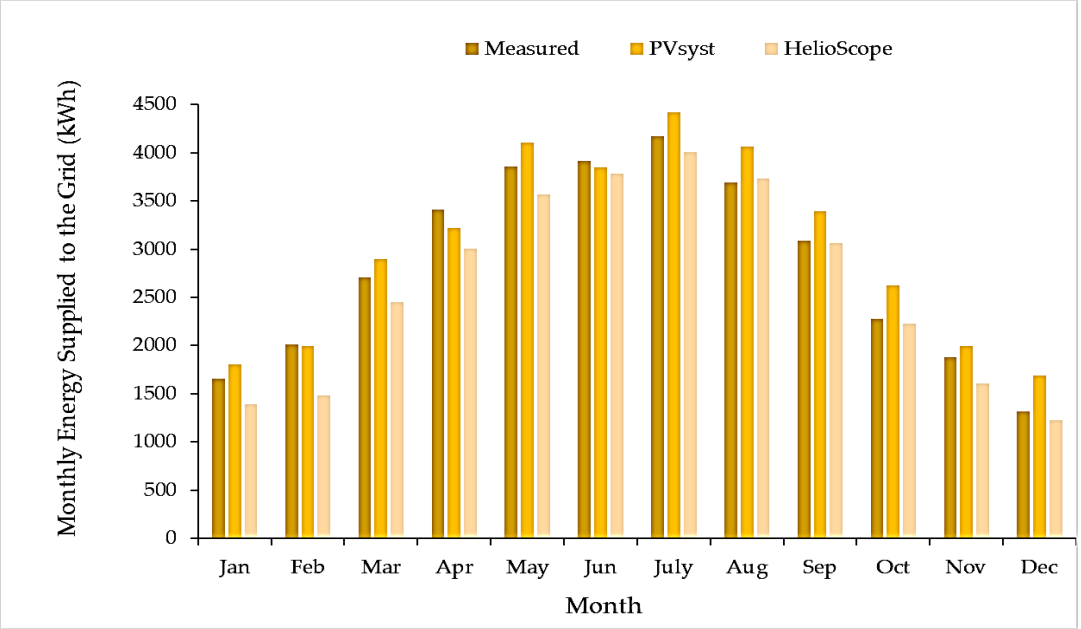


Figure 12. Monthly Average Measured and Simulated Energy Supplied to the Grid.

The annual measured energy yield is approximately 34.3 MWh, whereas PVsyst and HelioScope estimate annual productions of 36.3 MWh and 32.6 MWh, respectively. Accordingly, PVsyst overestimates the measured production by approximately 2.0 MWh (5–6%), while HelioScope underestimates it by about 1.7 MWh (5%). The fact that the measured value lies between the two simulated results suggests that the Meteonorm-based modeling approach provides a reasonable representation of the actual site conditions.

An analysis of monthly deviations indicates that PVsyst tends to generate higher production estimates, particularly during late summer and winter months. For instance, in August, the measured production of 3688.4 kWh is exceeded by the PVsyst estimate of 4067 kWh, resulting in a difference of 379 kWh, while in October this deviation reaches 348 kWh. In contrast, the discrepancy in June is limited to 68 kWh, indicating a closer agreement during mid-summer. HelioScope, conversely, produces generally more conservative estimates, with pronounced underestimations observed in February (526 kWh) and April (411 kWh), whereas a very close agreement is achieved in September (23 kWh).

From a seasonal perspective, the measured energy production during the summer period (May–August) amounts to approximately 15.6 MWh, compared to 16.6 MWh estimated by PVsyst and 15.3 MWh by HelioScope. During the winter period (December–February), the measured total production is approximately 5.0 MWh, while PVsyst and HelioScope predict 5.5 MWh and 4.1 MWh, respectively. These results indicate improved agreement between measured and simulated data during summer months, whereas larger deviations occur in winter due to increased meteorological uncertainty.

Overall, both PVsyst and HelioScope demonstrate acceptable accuracy in representing system performance. However, PVsyst exhibits a tendency to overestimate energy production, particularly in August and December, whereas HelioScope adopts a more conservative approach, especially in February and April. Consequently, PVsyst appears more suitable for upper-bound performance assessments, while HelioScope is better suited for conservative evaluations and financial risk analyses.

The measured and simulated performance parameters of the 24 kWp grid-connected PV system are presented in Table 11 to enable a direct comparison.

Table 11. Comparison of Measured and Simulated Performance of a 24 kWp Solar PV System.

Parameters	PVSyst	HelioScope		Measured	Relative Deviation * (%)		
	Meteonorm (a)	TSMS (b)	Meteonorm (c)		(a)	(b)	(c)
Annual global horizontal irradiance (kWh/m²)	1800.2	1703.4	1665.8	1603.7	12.3	6.2	3.9
In-plane irradiance (kWh/m²)	1908.2	1770.2	1705.6	1864	2.4	5.0	8.5
Effective irradiance on the collector plane (kWh)	220,950	206,810	200,560	223,680	1.2	7.5	10.3
PV efficiency at STC (%)	20.02	20.02	20.02	20.06	0.2	0.2	0.2
Array nominal energy at STC (kWh)	44,240	41,400	40,140	44,870	1.4	7.7	10.5
PV loss (%)							
Irradiance loss	0.6	0.7	1.2	1.8	66.7	61.1	33.3
Mismatch loss	2.1	2.8	2.8	2.0	5.0	40.0	40.0
Soiling loss	3.0	2.0	2	2.5	20.0	20.0	20.0
Ohmic loss	1.4	0.5	1	1.8	22.2	72.2	44.4
Temperature loss	4.1	11.2	8.5	10.8	62.0	3.7	21.3
Inverter loss (%)	5.2	4.9	4.9	5.4	3.7	9.3	9.3
Energy to grid (kWh)	36,049	32,173.5	31,544	33,977.5	6.1	5.3	7.2
PR (%)	78.7	76.4	77.1	75.7	4.0	0.9	1.8

* Absolute relative deviation calculated as (|Measured − Simulated|/Simulated) × 100.

4. Discussion

In this study, the performance of a 24 kWp grid-connected rooftop PV system installed in Yeşilova was monitored throughout the year 2024. The annual performance parameters were empirically measured and subsequently compared with simulation data generated via PVSyst and HelioScope software. Regarding energy yield analysis, the HelioScope simulation supported by TSMS data demonstrated the highest degree of congruence with the actual production values. Conversely, significant deviations were observed when utilizing the Meteonorm dataset; specifically, PVSyst overestimated the annual total energy yield by 5.74%, whereas HelioScope exhibited an underestimation of 7.18%.

The observed discrepancies between PVsyst and HelioScope suggest that the 'modeling gap' is not merely a software limitation but is deeply linked to the sensitivity of algorithms and numerical solvers to local meteorological inputs. Specifically, the divergence in winter performance predictions (e.g., the 17.1% deviation in January) can be attributed to how different transposition models handle diffuse radiation at low sun angles. According to the foundational daylight and irradiance component models proposed by Perez et al. [90] and the extensive model validations for tilted planes conducted by Ineichen [91], the choice between anisotropic (Perez) and isotropic (Hay) sky models significantly impacts the estimation of circumsolar and horizon brightening components. This variation is further compounded by the different 'numerical solvers' used for incident angle modifier (IAM) calculations and the empirical 'u-value' thermal loss coefficients, which dictate how each software interprets convective cooling under fluctuating local wind speeds. Furthermore, the convergence criteria of the software's internal energy balance engines and their handling of hourly vs. sub-hourly time steps influence the accuracy of clipping and shading losses. The overestimation in PVSyst likely stems from its idealized spectral loss model, which may not fully capture the local atmospheric aerosol levels in the Yeşilova region compared to the ground-measured TSMS data.

In terms of the PR, the recorded annual value of 75.7% confirms that the system's component efficiency and operational quality align with global standards. This ratio significantly outperforms reported yields from various geographies, including Ireland (54.0–60.0%), Greece (67.36%), and Indonesia (60.0%). Although the observed PR is slightly

lower than specific high-efficiency studies focusing on advanced technologies, such as bifacial modules, in Portugal (85.5%) and the USA (84.0%), the results remain near the upper threshold of the internationally accepted 60–80% range for grid-connected PV systems.

The correlation between energy production and PR data reveals that the higher results produced by simulation tools (PVSyst: 78.7%; HelioScope: 77.1%) relative to the measured PR are consistent with the 'idealized loss modeling' trend. This tracking error between simulation and reality is primarily driven by the component models for thermal loss. While simulations often assume a constant heat loss coefficient, the empirical data shows that dynamic wind-driven cooling and the specific mounting geometry of the rooftop installation create non-linear thermal behaviors that standard NOCT-based models fail to interpret fully during peak summer months. Notably, the fact that HelioScope achieved a marginal deviation of only 1.85% from the empirical data indicates its superior capability in accurately modeling local thermal losses and system-specific technical variables. Consequently, the annual energy output, bolstered by a high PR, validates that the Yeşilova region possesses significant techno-economic potential for solar energy investments.

The key performance outcomes of the 24 kWp grid-connected PV system are summarized as follows:

- Generation variability: The system exhibited significant seasonal variation, reaching a peak monthly energy production of 4173.60 kWh in July 2024, whereas the minimum output was recorded in December 2024 at 1314.40 kWh.
- Yield parameters: The annual average daily array yield was determined to be 4.64 h/d, operating against a reference yield of 5.09 h/d.
- Efficiency metrics: The PV installation demonstrated robust performance with an annual PR of 75.7% and a CF of 16.99%.
- Loss analysis and interpretation: System losses remained within optimized limits, and the specific breakdown of annual loss components—including thermal capture losses, miscellaneous capture losses, and inverter-related efficiencies—is presented in detail in Table 11. The various negative capture losses (L_{CM}) shown in Table 6, observed during the summer months, are primarily attributed to the inherent limitations and measurement uncertainties of thermal modeling. Specifically, NOCT-derived temperature estimation algorithms often fail to fully capture dynamic convective cooling effects in the Mediterranean climate, while potential inaccuracies in plane-of-array irradiance measurements during peak solar periods can introduce mathematical deviations [87,88]. Furthermore, the interpretation of these differences reveals that inverter efficiency models in simulations often overlook low-load efficiency drops during early morning and late evening time steps, leading to a minor over-prediction of conversion efficiency.
- Simulation deviation and practitioner benchmarking: Comparative analysis revealed that utilizing Meteonorm data led to diverging results; PVSyst overestimated the annual yield by 5.74%, while HelioScope underestimated it by 7.18%. We have expanded our analysis to interpret these software discrepancies as a "benchmarking reference" for practitioners to balance computational burden with predictive reliability, emphasizing that high-fidelity models must prioritize site-specific TSMS data over synthetic datasets.
- Data source reliability: The energy yield predictions generated by HelioScope using TSMS-derived meteorological data showed the highest degree of convergence with the actual measured values.
- Global benchmarking: The recorded PR of 75.7% validates that the system's component efficiency and operational quality are consistent with high-tier international standards.

- Software validation and PR correlation: The higher PR estimates provided by PVSyst (78.7%) and HelioScope (77.1%) align with the "idealized loss modeling" trend prevalent in existing literature.
- Model accuracy: HelioScope demonstrated superior modeling accuracy for this specific site, with a marginal 1.85% deviation from the measured PR. This suggests that HelioScope's internal numerical solvers for thermal variations and its specific component models for the selected inverter–module pair were better calibrated for the local climate than PVSyst's default parameters.

5. Conclusions

This study develops a comprehensive decision-support framework and benchmarking protocol for PV energy modeling that systematically evaluates the trade-offs between model complexity and predictive accuracy relative to defined acceptance criteria. Based on the one-year empirical monitoring of the 24 kWp system in Yeşilova, the following conclusions are drawn:

- Quantitative performance and benchmarking: The system demonstrated high operational reliability with an annual energy yield of 33,977.5 kWh, an average PR of 75.7%, and a CF of 16.99%. These results align with high-tier international standards and validate the region's solar potential. Comparative analysis showed that while HelioScope (using TSMS data) achieved a marginal PR deviation of only 1.85%, the use of synthetic Meteonorm data led to discrepancies of +5.74% in PVSyst and −7.18% in HelioScope, highlighting the critical importance of site-specific meteorological inputs over generalized datasets.
- Study limitations: Despite the robust validation, this study is subject to certain limitations. While irradiance was recorded at 1-min intervals, the reliance on hourly-averaged data for long-term simulations may not fully capture sub-minute irradiance volatility affecting real-time inverter efficiency. Additionally, standard thermal loss modeling (NOCT-based) struggled to account for non-linear convective cooling during high-wind summer periods in the Mediterranean climate, which remains a key source of modeling uncertainty.
- Risk mitigation and policy implications: By explicitly quantifying uncertainty in energy yield estimations, the framework not only supports technical model selection but also contributes to reducing financial risk exposure in distributed generation investments. From a policy perspective, improving predictive reliability is critical for enhancing investor confidence, refining feed-in tariff structures, and informing risk-adjusted return calculations central to bankability assessments.
- Future research directions: Logically following these results, future work will focus on high-frequency (1-s) measured-profile validation to interpret power quality indicators and ramp-rate reduction. Furthermore, integrating battery energy storage systems (BESSs) and applying advanced machine learning for real-time fault detection are proposed to enhance grid stability and participation in ancillary service markets. Detailed parameter sensitivity analysis (targeting albedo and soiling) and uncertainty quantification of sensor-to-model propagation are essential to refine the predictive reliability of digital twin models.

Overall, the integration of physics-based simulations, data-driven intelligence, and techno-economic evaluation provides a scalable foundation for evidence-based energy policy development. By linking modeling precision with financial risk mitigation and grid-level performance, this study supports more resilient, transparent, and economically sustainable PV deployment strategies.

Author Contributions: N.C.: project administration, investigation, visualisation, formal analysis, software, and writing—original draft; H.K.C.: conceptualisation, methodology, and resources; F.Ö.A.: visualisation, software, and data curation; A.E.W.R.: validation and writing—review and editing. All authors have read and agreed to the published version of the manuscript.

Funding: This research received no external funding.

Data Availability Statement: The original contributions presented in this study are included in the article. Further inquiries can be directed to the corresponding author.

Acknowledgments: The authors affirm that no generative artificial intelligence (AI) or AI-assisted technologies were employed in the production of this manuscript's content, with the sole exception of AI tools (ChatGPT 5.2) used for language refinement and grammatical editing.

Conflicts of Interest: The authors declare no conflicts of interest and have no known financial or personal affiliations that could have influenced the reported work. T

Abbreviations

The following abbreviations are used in this manuscript:

AEP	Annual energy produced
A_{PV}	Total area of PV array (m^2)
BESS	Battery energy storage systems
CAPEX	Capital expenditures
CF	Capacity utilisation factor (%)
Eac	AC energy output (kWh)
Edc	DC energy output (kWh)
E_{grid}	Energy supply to the grid (kWh)
EMRA	Energy Market Regulatory Authority
EU	European Union
GHI	Global horizontal irradiance
h/d	Hour/day
IAM	Incidence angle modifier
IEC	International Electrotechnical Commission (IEC 61724-1)
IEA	International Energy Agency
IRR	Internal rate of return
LCCA	Life-cycle cost analysis
LCE	Levelized Cost of Energy
LCOE	Levelized cost of energy
MENR	Ministry of Energy and Natural Resources
MPPT	Maximum power point tracking
NOCT	Nominal operating cell temperature
NPV	Net present value
NREL	National Renewable Energy Laboratory
POA	Plane of Array
PR	Performance ratio (%)
P_{rated}	Rated power of PV system (kWp)
PVPS	Photovoltaic Power Systems Programme
ROI	Return on investment
STC	Standard test condition
TSMS	Turkish State Meteorological Service
Ya	Array yield (h/d)
YEKA	Renewable Energy Resource Zone
Yf	Final yield (h/d)
Yr	Reference yield (h/d)

References

1. IEA. *World Energy Outlook 2024*; International Energy Agency: Paris, France, 2024. Available online: https://www.iea.org/reports/world-energy-outlook-2024 (accessed on 14 October 2025).
2. REN21. *Renewables 2024 Global Status Report*; Global Status Report Collection; REN21 Secretariat: Paris, France, 2024. Available online: https://www.ren21.net/reports/global-status-report/ (accessed on 5 February 2025).
3. IEA-PVPS. *Snapshot of Global PV Markets 2024*; Report IEA-PVPS T1-42:2024; International Energy Agency Photovoltaic Power Systems Programme: Paris, France, 2024. Available online: https://iea-pvps.org/wp-content/uploads/2024/04/Snapshot-of-Global-PV-Markets_2024.pdf (accessed on 11 February 2025).
4. IEA-PVPS. *Trends in Photovoltaic Applications 2024*; IEA-PVPS T1-41:2024; International Energy Agency Photovoltaic Power Systems Programme: Paris, France, 2024. Available online: https://iea-pvps.org/wp-content/uploads/2024/10/IEA-PVPS-Task-1-Trends-Report-2024.pdf (accessed on 11 February 2025).
5. Ember Climate. *European Electricity Review 2025*; Ember Climate: London, UK, 2025. Available online: https://ember-energy.org/app/uploads/2025/01/EER_2025_22012025.pdf (accessed on 11 February 2025).
6. Ember. Share of Electricity Generated by Solar Power. In *Energy Institute—Statistical Review of World Energy (2025)—with Major Processing by Our World in Data*; Ember: London, UK, 2026. Available online: https://archive.ourworldindata.org/20260128-110227/grapher/share-electricity-solar.html (accessed on 2 February 2026).
7. Republic of Türkiye Ministry of Energy and Natural Resources (MENR). *GEPA—Güneş Enerjisi Potansiyelimiz*; Republic of Türkiye Ministry of Energy and Natural Resources (MENR): Ankara, Türkiye, 2024. Available online: https://enerji.gov.tr/bilgi-merkezi-enerji-gunes (accessed on 15 October 2025). (In Türkish)
8. Demirkesen, S.; Variyenli, H.I. The Model of "Free Investment and Centralised Management" in Renewable Energy Production Projects. *Int. J. Energy Stud.* **2021**, *6*, 1–18.
9. Turkish Electricity Transmission Corporation (TEIAS). *Installed Capacity Reports by Energy Resource*; Turkish Electricity Transmission Corporation (TEIAS): Ankara, Türkiye, 2025. Available online: https://www.teias.gov.tr/en-US/electricity-transmission-in-turkiye (accessed on 2 February 2026).
10. Republic of Türkiye Ministry of Energy and Natural Resources (MENR). *News: Installed Power in Renewable Energy Exceeded 75 Thousand Megawatts*; Republic of Türkiye Ministry of Energy and Natural Resources (MENR): Ankara, Türkiye, 2026. https://enerji.gov.tr/news-detail?id=31682 (accessed on 2 February 2026).
11. Ember. *Total Installed Capacity in Türkiye*; Ember Energy: London, UK, 2025. Available online: https://ember-energy.org/data/turkiye-electricity-data-tools/ (accessed on 2 February 2026).
12. Republic of Türkiye Ministry of Energy and Natural Resources. *YEKA Renewable Energy Resource Areas Program Overview*; Republic of Türkiye Ministry of Energy and Natural Resources: Ankara, Türkiye, 2024. Available online: https://enerji.gov.tr/production-activities-en (accessed on 2 April 2025).
13. Republic of Türkiye Ministry of Energy and Natural Resources. *Türkiye Energy Transition and 2035 Renewable Energy Roadmap*; Renewable Energy 2035 Roadmap; Republic of Türkiye Ministry of Energy and Natural Resources: Ankara, Türkiye, 2024. Available online: https://enerji.gov.tr/Media/Dizin/BHIM/tr/Duyurular/Lansman%20EN_202410221149.pdf (accessed on 2 April 2025).
14. Ministry of Energy and Natural Resources (MENR). *Türkiye National Energy Plan*; Ministry of Energy and Natural Resources (MENR): Ankara, Türkiye, 2022. https://enerji.gov.tr/Media/Dizin/EIGM/tr/Raporlar/TUEP/T%C3%BCrkiye_National_Energy_Plan.pdf (accessed on 5 July 2025).
15. Anadolu Agency. Economy. *Türkiye Announces National Energy Plan and Hydrogen Strategy*; Anadolu Agency: Ankara, Türkiye, 2025. Available online: https://www.aa.com.tr/en/economy/turkiye-announces-national-energy-plan-and-hydrogen-strategy/2791948 (accessed on 15 March 2025).
16. Ates, A.M.; Singh, H. Rooftop solar Photovoltaic (PV) Plant—One Year Measured Performance and Simulations. *J. King Saud Univ. Sci.* **2021**, *33*, 101361. https://doi.org/10.1016/j.jksus.2021.101361.
17. Dindar, T.; Esen, V.; Sarkın, A.S. Comparison of Simulation Results for 25 kW Power Output Rooftop PV System. *Eur. J. Tech.* **2022**, *12*, 282–291. https://doi.org/10.36222/ejt.1175023.
18. Ibrahim, I.M.; Shehata, A.S.; Shehata, A.I.; Mohamed, A. Performance Analysis of 10 MWp Grid-Connected Photovoltaic System in The Mediterranean Climate Using PVsyst Software. *Int. J. Smart Grid Clean Energy* **2021**, *10*, 286–291. https://doi.org/10.12720/sgce.10.4.286-291.

19. Villa-Ávila, E.; Arévalo, P.; Ochoa-Correa, D.; Villa-Ávila, M.; Sempértegui-Moscoso, E.; Jurado, F. A New Methodology for Estimating the Potential for Photovoltaic Electricity Generation on Urban Building Rooftops for Self-Consumption Applications. *Smart Cities* **2024**, *7*, 3798–3822. https://doi.org/10.3390/smartcities7060146.
20. Benavides, D.; Arévalo, P.; Ortega, A.C.; Sánchez-Sutil, F.; Villa-Ávila, E. Energy Management Model for a Remote Microgrid Based on Demand-Side Energy Control. *Energies* **2024**, *17*, 170. https://doi.org/10.3390/en17010170.
21. Sancar, M.R.; Bayram, A.B. Modeling and Economic Analysis of Greenhouse Top Solar Power Plant with Pvsyst Software. *Int. J. Eng. Innov. Res.* **2023**, *5*, 48–59. https://doi.org/10.47933/ijeir.1209362.
22. Ulgen, K.; Hepbasli, A. Comparison of Solar Radiation Correlations for Izmir, Turkey. *Int. J. Energy Res.* **2002**, *26*, 413–430. https://doi.org/10.1002/er.794.
23. González-Peña, D.; García-Ruiz, I.; Díez-Mediavilla, M.; Dieste-Velasco, M.I.; Alonso-Tristán, C. Photovoltaic Prediction Software: Evaluation with Real Data from Northern Spain. *Appl. Sci.* **2021**, *11*, 5025. https://doi.org/10.3390/app11115025.
24. Skoplaki, E.; Palyvos, J.A. On The Temperature Dependence of Photovoltaic Module Electrical Performance: A Review of Efficiency/Power Correlations. *Sol. Energy* **2009**, *83*, 614–624. https://doi.org/10.1016/j.solener.2008.10.008.
25. PVsyst, SA. *PVsyst Photovoltaic System Simulation Software*; PVsyst, SA: Satigny, Switzerland, 2025. Available online: https://www.pvsyst.com (accessed on 10 June 2025).
26. HelioScope. *HelioScope Photovoltaic System Design Software*; Folsom Labs, LLC: San Francisco, CA, USA, 2025. Available online: https://www.helioscope.com (accessed on 10 June 2025).
27. Thevenard, D.; Pelland, S. Estimating the Uncertainty in Long-Term Photovoltaic Yield Predictions. *Sol. Energy* **2013**, *91*, 432–445. https://doi.org/10.1016/j.solener.2011.05.006.
28. Makrides, G.; Zinsser, B.; Schubert, M.; Georghiou, G.E. Energy Yield Prediction Errors and Uncertainties of Different Photovoltaic Models. *Prog. Photovolt. Res. Appl.* **2013**, *21*, 500–516. https://doi.org/10.1002/pip.1218.
29. Abbasoğlu, S.; Babatunde, A.A. Evaluation of field data and simulation results of a photovoltaic system in countries with high solar radiation. *Turk. J. Electr. Eng. Comput. Sci.* **2015**, *23*, 1608–1618. https://doi.org/10.3906/elk-1402-313.
30. Zgham, W.; Shirzad, S.; Fatemi, S.A.Z. Energy Assessment & Comparative Study of Mono and Poly Solar PV Technologies Using Advanced PVsyst Software. *Arch. Adv. Eng. Sci.* **2024**, 1–7. https://doi.org/10.47852/bonviewAAES42021881.
31. Baqir, M.; Channi, H.K. Analysis and Design of Solar PV System Using Pvsyst Software. *Mater. Today Proc.* **2022**, *48*, 1332–1338. https://doi.org/10.1016/j.matpr.2021.09.029.
32. Baviskar, S.; Patil, G.B.; Beldar, R. Predictive Analysis of 50 kW Solar Photovoltaic System Using PVsyst. In *Proceedings of the 2024 International Conference on Intelligent and Innovative Technologies in Computing, Electrical and Electronics (IITCEE)*; IEEE: New York, NY, USA, 2024; pp. 1–4. https://doi.org/10.1109/IITCEE59897.2024.10467946.
33. Mishra, P.R.; Rathore, S.; Jain, V. PVSyst Enabled Real Time Evaluation of Grid Connected Solar Photovoltaic System. *Int. J. Inf. Technol.* **2024**, *16*, 745–752. https://doi.org/10.1007/s41870-023-01677-x.
34. Kumar, R.; Rajoria, C.S.; Sharma, A.; Suhag, S. Design And Simulation of Standalone Solar PV System Using PVsyst Software: A Case Study. *Mater. Today Proc.* **2021**, *46*, 5322–5328. https://doi.org/10.1016/j.matpr.2020.08.785.
35. Kymakis, E.; Kalykakis, S.; Papazoglou, T.M. Performance Analysis of A Grid Connected Photovoltaic Park on The Island of Crete. *Energy Convers. Manag.* **2009**, *50*, 433–438. https://doi.org/10.1016/j.enconman.2008.12.009.
36. Saka, K.; Orhan, M.F. Performance Assessment and Useful Solar Radiation Analysis of a Grid-Connected Photovoltaic Plant in Türkiye. *Case Stud. Therm. Eng.* **2025**, *73*, 106565. https://doi.org/10.1016/j.csite.2025.106565.
37. Eksi, M.; Akarsu, R.T.; Ozcan, M. Net-zero Energy Building Transformation: Techno-economic and Environmental Evaluation in The Mediterranean Region. *Environ. Dev. Sustain.* **2025**, 1–41. https://doi.org/10.1007/s10668-025-06389-9.
38. Islam, M.M.; Kowsar, A.; Haque, A.K.M.M.; Hossain, M.K.; Ali, H.; Rubel, M.H.K.; Rahman, F. Techno-economic Analysis of Hybrid Renewable Energy System for Healthcare Centre in Northwest Bangladesh. *Process Integr. Optim. Sustain.* **2023**, *7*, 315–328. https://doi.org/10.1007/s41660-022-00294-8.
39. Ahmed, W.; Sheikh, J.A.; Nouman, M.; Ullah, M.F.; Mahmud, M.P. Techno-economic Analysis for The Role of Single End Energy User in Mitigating GHG Emission. *Energy Sustain. Soc.* **2021**, *11*, 32. https://doi.org/10.1186/s13705-021-00307-3.
40. *IEC 60751*; Industrial Platinum Resistance Thermometers and Platinum Temperature Sensors. International Electrotechnical Commission: Geneva, Switzerland, 2022.
41. *IEC Standard 61724*; IEC Photovoltaic System Performance Monitoring—Guidelines for Measurement, Data Exchange and Analysis. IEC: Geneva, Switzerland, 1998. Available online: https://webstore.iec.ch/en/publication/65561 (accessed on 15 June 2025).
42. Goel, S.; Sharma, R. Analysis of Measured and Simulated Performance of a Grid-Connected PV System in Eastern India. *Environ. Dev Sustain.* **2021**, *23*, 451–476. https://doi.org/10.1007/s10668-020-00591-7.

43. Long, C.N.; Dutton, E.G. BSRN Global Network Recommended QC Tests, V2.0, BSRN Technical Report. Available online: https://hdl.handle.net/10013/epic.38770.d001 (accessed on 6 March 2026).
44. Muneer, T. *Solar Radiation and Daylight Models for the Energy Efficient Design of Buildings*, 2nd ed.; Butterworth-Heinemann: London, UK, 2004. Available online: https://api.taylorfrancis.com/content/books/mono/download?identifierName=doi&identifierValue=10.4324/9780080474410&type=googlepdf (accessed on 6 March 2026).
45. Hoff, T.E.; Perez, R. Modeling PV fleet output variability. *Sol. Energy* **2012**, *86*, 2177–2189. https://doi.org/10.1016/j.solener.2011.11.005.
46. Stein, J.; Hansen, C.; Reno, M.J. *The Variability Index: A New and Novel Metric for Quantifying Irradiance and PV Output Variability*; (No. SAND2012-2088C); Sandia National Laboratories: Albuquerque, NM, USA, 2012.
47. Díez-Mediavilla, M.; Alonso-Tristán, C.; Rodríguez-Amigo, M.C.; García-Calderón, T.; Dieste-Velasco, M.I. Performance Analysis of PV Plants: Optimization for Improving Profitability. *Energy Convers. Manag.* **2012**, *54*, 17–23. https://doi.org/10.1016/j.enconman.2011.09.013.
48. Tian, W.; Wang, Y.; Ren, J.; Zhu, L. Effect of Urban Climate on Building Integrated Photovoltaics Performance. *Energy Convers Manag.* **2007**, *48*, 1–8. https://doi.org/10.1016/j.enconman.2006.05.015.
49. Maghami, M.R.; Hizam, H.; Gomes, C.; Radzi, M.A.; Rezadad, M.I.; Hajighorbani, S. Power Loss Due to Soiling on Solar Panel: A Review. *Renew Sustain Energy Rev.* **2016**, *59*, 1307–1316. https://doi.org/10.1016/j.rser.2016.01.044.
50. Silvestre, S.; Chouder, A.; Karatepe, E. Automatic Fault Detection in Grid Connected PV Systems. *Sol. Energy* **2013**, *94*, 119–127. https://doi.org/10.1016/j.solener.2013.05.001.
51. Cubukcu, M.; Gumus, H. Performance Analysis of a Grid-Connected Photovoltaic Plant in Eastern Turkey. *Sustain. Energy Technol. Assess.* **2020**, *39*, 100724. https://doi.org/10.1016/j.seta.2020.100724.
52. de Lima, L.C.; de Araújo Ferreira, L.; de Lima Morais, F.H.B. Performance Analysis of a Grid Connected Photovoltaic System in Northeastern Brazil. *Energy Sustain. Develop.* **2017**, *37*, 79–85. https://doi.org/10.1016/j.esd.2017.01.004.
53. Mondol, J.D.; Yohanis, Y.; Smyth, M.; Norton, B. Long Term performance Analysis of a Grid Connected Photovoltaic System in Northern Ireland. *Energy Convers. Manag.* **2006**, *47*, 2925–2947. https://doi.org/10.1016/j.enconman.2006.03.026.
54. Bolson, N.; Prieto, P.; Patzek, T. Capacity Factors for Electrical Power Generation from Renewable and Nonrenewable Sources. *Proc. Natl. Acad. Sci. USA* **2022**, *119*, e2205429119. https://doi.org/10.1073/pnas.2205429119.
55. Iturralde Carrera, L.A.; Garcia-Barajas, M.G.; Constantino-Robles, C.D.; Álvarez-Alvarado, J.M.; Castillo-Alvarez, Y.; Rodríguez-Reséndiz, J. Efficiency and Sustainability in Solar Photovoltaic Systems: A Review of Key Factors and Innovative Technologies. *Eng* **2025**, *6*, 50. https://doi.org/10.3390/eng6030050.
56. Dubey, S.; Sarvaiya, J.N.; Seshadri, B. Temperature dependent photovoltaic (PV) efficiency and its effect on PV production in the world—A review. *Energy Procedia* **2013**, *33*, 311–321. https://doi.org/10.1016/j.egypro.2013.05.072.
57. Yadav, S.K.; Bajpai, U. Performance Evaluation of a Rooftop Solar Photovoltaic Power Plant in Northern India. *Energy Sustain. Dev.* **2018**, *43*, 130–138. https://doi.org/10.1016/j.esd.2018.01.006.
58. Santiago, I.; Trillo Montero, D.; Luna Rodriguez, J.J.; Moreno Garcia, I.M.; Palacios Garcia, E.J. Graphical Diagnosis of Performances in Photovoltaic Systems: A Case Study in Southern Spain. *Energies* **2017**, *10*, 1964. https://doi.org/10.3390/en10121964.
59. Mulcué-Nieto, L.F.; Mora-López, L. A New Model to Predict The Energy Generated by a Photovoltaic System Connected to the Grid in Low Latitude Countries. *Sol. Energy* **2014**, *107*, 423–442. https://doi.org/10.1016/j.solener.2014.04.030.
60. Fernández-Solas, Á.; Montes-Romero, J.; Micheli, L.; Almonacid, F.; Fernández, E.F. Estimation of Soiling Losses in Photovoltaic Modules of Different Technologies Through Analytical Methods. *Energy* **2022**, *244*, 123173. https://doi.org/10.1016/j.energy.2022.123173.
61. John, J.J. Characterization of Soiling Loss on Photovoltaic Modules, and Development of a Novel Cleaning System. Ph.D. Thesis, Indian Institute of Technology Bombay, Mumbai, India, 2015. Available online: https://www.ee.iitb.ac.in/~anilkg/Jim-thesis.pdf?utm_source=chatgpt.com (accessed on 3 February 2026).
62. Muller, M. *Development of a Novel Soiling Chamber for Testing Antisoiling Coatings*; No. NREL/CP-5K00-82578; National Renewable Energy Lab. (NREL): Golden, CO, USA, 2023. Available online: https://www.nrel.gov/docs/fy23osti/82578.pdf (accessed on 3 February 2026).
63. Ilse, K.K.; Figgis, B.W.; Naumann, V.; Hagendorf, C.; Bagdahn, J. Fundamentals of Soiling Processes on Photovoltaic Modules. *Renew. Sustain. Energy Rev.* **2018**, *98*, 239–254. https://doi.org/10.1016/j.rser.2018.09.015.
64. Borah, P.; Micheli, L.; Sarmah, N. Analysis of Soiling Loss in Photovoltaic Modules: A Review of the Impact of Atmospheric Parameters, Soil Properties, and Mitigation Approaches. *Sustainability* **2023**, *15*, 16669. https://doi.org/10.3390/su152416669.

65. Wurster, T.S.; Schubert, M.B. Mismatch Loss in Photovoltaic Systems. *Sol. Energy* **2014**, *105*, 505–511. https://doi.org/10.1016/j.solener.2014.04.014.
66. Smith, R.M.; Matam, M.; Seigneur, H. Mismatch Losses in a PV System Due to Shortened Strings. *Energy Convers. Manag.* **2021**, *250*, 114891. https://doi.org/10.1016/j.enconman.2021.114891.
67. Mansur, A.A.; Amin, M.R.; Islam, K.K. Performance comparison of mismatch power loss minimization techniques in series-parallel PV array configurations. *Energies* **2019**, *12*, 874. https://doi.org/10.3390/en12050874.
68. Gostein, M.; Caron, J.R.; Littmann, B. Measuring Soiling Losses at Utility-scale PV Power Plants. In *Proceedings of the 2014 IEEE 40th Photovoltaic Specialist Conference (PVSC)*; IEEE: New York, NY, USA, 2014; pp. 0885–0890. https://doi.org/10.1109/PVSC.2014.6925056.
69. Deceglie, M.G.; Micheli, L.; Muller, M. Quantifying Soiling Loss Directly from PV Yield. *IEEE J. Photovolt.* **2018**, *8*, 547–551. https://doi.org/10.1109/JPHOTOV.2017.2784682.
70. Matula, R.A. Electrical Resistivity of Copper, Gold, Palladium, and Silver. *J. Phys. Chem. Ref. Data* **1979**, *8*, 1147–1298. https://doi.org/10.1063/1.555614.
71. Branker, K.; Pathak, M.J.M.; Pearce, J.M. A Review of Solar Photovoltaic Levelized Cost of Electricity. *Renew. Sustain. Energy Rev.* **2011**, *15*, 4470–4482. https://doi.org/10.1016/j.rser.2011.07.104.
72. Reddy, V.R.; Kurian, M.; Ardakanian, R. Life-cycle Cost Approach (LCCA): Framework and Concepts. In *Life-Cycle Cost Approach for Management of Environmental Resources: A Primer*; Springer International Publishing: Cham, Switzerland, 2014; pp. 17–37. https://doi.org/10.1007/978-3-319-06287-7_2.
73. Darling, S.B.; You, F.; Veselka, T.; Velosa, A. Assumptions and the Levelized Cost of Energy for Photovoltaics. *Energy Environ. Sci.* **2011**, *4*, 3133–3139. https://doi.org/10.1039/C0EE00698J.
74. Somasundaram, S.; Tay, A.A.O. Performance Study and Economic Analysis of Photovoltaic Thermal System Under Real-life Thermal Loads in Tropical Climate. *Sustain. Environ. Res.* **2019**, *29*, 34. https://doi.org/10.1186/s42834-019-0040-5.
75. Tomczyk, D.; Łapniewska, Z. Solar Panels on Every Rooftop? Photovoltaics Boom in Poland and the Role of the European Union funds. *Energy Res. Soc. Sci.* **2025**, *125*, 104107. https://doi.org/10.1016/j.erss.2025.104107.
76. Buyukbicakci, E. Geographic and Thermal Impact on the Performance of Hybrid PV–TE Energy Systems. *Sci. Rep.* **2025**, *15*, 40169. https://doi.org/10.1038/s41598-025-23850-x.
77. Tahir, Z.R.; Kanwal, A.; Asim, M.; Bilal, M.; Abdullah, M.; Saleem, S.; Mujtaba, M.A.; Veza, I.; Mousa, M.; Kalam, M.A. Effect of Temperature and Wind Speed on Efficiency of Five Photovoltaic Module Technologies for Different Climatic Zones. *Sustainability* **2022**, *14*, 15810. https://doi.org/10.3390/su142315810.
78. Shaw, V.K. Predicting Solar Potential: A Comprehensive Analysis of On-Grid Rooftop Solar PV System through HelioScope Design. *Int. J. Res. Appl. Sci. Eng. Technol.* **2023**, *11*, 244–255. https://doi.org/10.22214/ijraset.2023.55970.
79. Pietruszko, S.M.; Gradzki, M. Performance of a Grid Connected Small PV System in Poland. *Appl Energy* **2003**, *74*, 177–184. https://doi.org/10.1016/S0306-2619(02)00144-7.
80. Sharma, V.; Chandel, S.S. Performance Analysis of a 190 kWp Grid Interactive Solar Photovoltaic Power Plant in India. *Energy* **2013**, *55*, 476–485. https://doi.org/10.1016/j.energy.2013.03.075.
81. Leloux, J.; Narvarte, L.; Trebosc, D. Review of the Performance of Residential PV systems in France. *Renew. Sustain. Energy Rev.* **2012**, *16*, 1369–1376. https://doi.org/10.1016/J.RSER.2011.10.018.
82. Milan, H.F.; Alves, A.Q.; Souza, T.A.; Galo, J.M.; Maia, A.S.; Borges, M.A.; Egoavil, C.J. The PV Performance Ratio Paradox: Annual Data from Large-scale, Real-world PV Systems Show Negligible Meteorological and Technical Impact and Points to Dominant Human Factors. *arXiv* **2025**, https://doi.org/10.48550/arXiv.2511.16834.
83. Sharma, R.; Goel, S. Performance Analysis of a 11.2 kWp Roof Top Grid-Connected PV System in Eastern India. *Energy Rep.* **2017**, *3*, 76–84. https://doi.org/10.1016/j.egyr.2017.05.001.
84. Matiyali, K.K.; Ashok, A. Performance Evaluation of Grid Connected Solar PV Power Plant. In Proceedings of the 2nd International Conference on Advances in Computing, Communication, & Automation (ICACCA) (Fall), Bareilly, India, 30 September –1 October 2016; pp. 1–5. https://doi.org/10.1109/ICACCAF.2016.7748989.
85. Shukla, A.K.; Sudhakar, K.; Baredar, P. Simulation and Performance Analysis of 110 kWp Grid-Connected Photovoltaic System for Residential Building in India: A Comparative Analysis of Various PV Technology. *Energy Rep.* **2016**, *2*, 82–88. https://doi.org/10.1016/j.egyr.2016.04.001.
86. Faiman, D. Assessing the Outdoor Operating Temperature of Photovoltaic Modules. *Prog. Photovolt. Res. Appl.* **2008**, *16*, 307–315. https://doi.org/10.1002/pip.813.

87. King, D.L.; Kratochvil, J.A.; Boyson, W.E. *Measuring Solar Spectral and Angle-of-Incidence Effects on Photovoltaic Modules and Solar Irradiance Sensors*; Sandia National Laboratories Report SAND2004-3535; Sandia National Laboratories: Albuquerque, NM, USA, 2004. Available online: https://www.osti.gov/servlets/purl/548689 (accessed on 4 February 2026).
88. Vårnes, A.M. Performance Assessment of a Solar PV-Grid Connected Installation in Ås, Norway. Master's Thesis, Norwegian University of Life Sciences, Ås, Norway, 2014. Available online: https://static02.nmbu.no/mina/studier/moppgaver/2014-Vagnes.pdf (accessed on 4 February 2026).
89. Chouder, A.; Silvestre, S. Automatic Supervision and Fault Detection of PV Systems Based on Power Losses Analysis. *Energy Convers. Manag.* **2010**, *51*, 1929–1937. https://doi.org/10.1016/j.enconman.2010.02.025.
90. Perez, R.; Ineichen, P.; Seals, R.; Michalsky, J.; Stewart, R. Modeling Daylight Availability and Irradiance Components From Direct and Global Irradiance. *Sol. Energy* **1990**, *44*, 271–289.
91. Ineichen, P. *Global Irradiance on Tilted and Oriented Planes: Model Validations*; Technical Report; University of Geneva: Geneva, Switzerland, 2011; pp. 1-78. Available online: https://archive-ouverte.unige.ch/unige:23519 (accessed on 4 February 2026).

Disclaimer/Publisher's Note: The statements, opinions and data contained in all publications are solely those of the individual author(s) and contributor(s) and not of MDPI and/or the editor(s). MDPI and/or the editor(s) disclaim responsibility for any injury to people or property resulting from any ideas, methods, instructions or products referred to in the content.